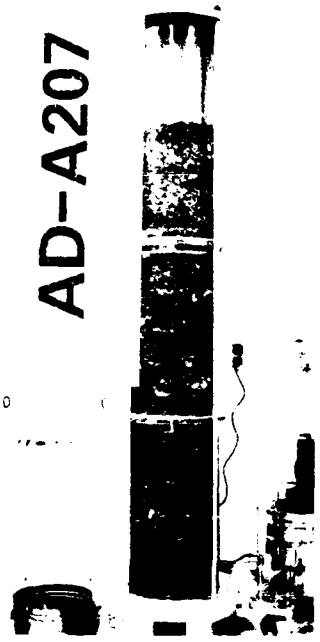

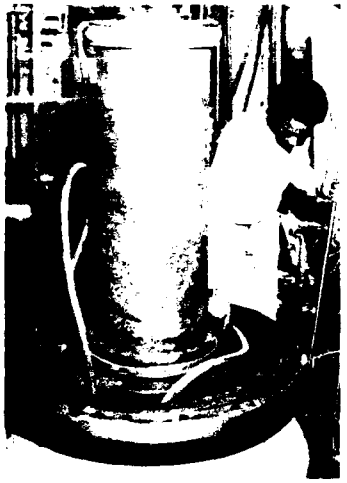

MISCELLANEOUS PAPER GL-89-5

STUDY OF EMBANKMENT PERFORMANCE DURING OVERTOPPING AND THROUGHFLOW

Report 2
HYDRAULIC STUDY AND MODELING OF MODELS

by

Hon-Yim Ko, R. Jeffrey Dunn, Ebrahim Simantob

University of Colorado
Boulder, Colorado 80302

April 1989
Report 2 of a Series

Prepared for DEPARTMENT OF THE ARMY
US Army Corps of Engineers
Washington, DC 20314-1000

Under Contract No. DACW39-83-C-0011

Destroy this report when no longer needed. Do not return it to the originator.

The findings in this report are not to be construed as an official Department of the Army position unless so designated by other authorized documents.

The contents of this report are not to be used for advertising, publication, or promotional purposes. Citation of trade names does not constitute an official endorsement or approval of the use of such commercial products.

REPORT DOCUMENTATION PAGE

Form Approved OMB No. 0704-0188

1a REPORT SECURITY CLASSIFICATION: Unclassified	1b RESTRICTIVE MARKINGS:
2a SECURITY CLASSIFICATION AUTHORITY:	3 DISTRIBUTION/AVAILABILITY OF REPORT: Approved for public release; distribution unlimited.
2b DECLASSIFICATION/DOWNGRADING SCHEDULE:	
4 PERFORMING ORGANIZATION REPORT NUMBER(S):	5 MONITORING ORGANIZATION REPORT NUMBER(S): Miscellaneous Paper GL-89-5
6a NAME OF PERFORMING ORGANIZATION: University of Colorado; 6b OFFICE SYMBOL (If applicable):	7a NAME OF MONITORING ORGANIZATION: USAEWES Geotechnical Laboratory
6c ADDRESS (City, State, and ZIP Code): Boulder, CO 80302	7b ADDRESS (City, State, and ZIP Code): PO Box 631 Vicksburg, MS 39181-0631
8a NAME OF FUNDING/SPONSORING ORGANIZATION: US Army Corps of Engineers; 8b OFFICE SYMBOL (If applicable):	9 PROCUREMENT INSTRUMENT IDENTIFICATION NUMBER: Contract No. DACW39-83-C-0011
8c ADDRESS (City, State, and ZIP Code): Washington, DC 20314-1000	10 SOURCE OF FUNDING NUMBERS: PROGRAM ELEMENT NO; PROJECT NO; TASK NO; WORK UNIT ACCESSION NO

11 TITLE (Include Security Classification)
Study of Embankment Performance During Overtopping and Throughflow, Report 2, Hydraulic Study and Modeling of Models

12 PERSONAL AUTHOR(S)
Ko, Hon-Yim, Dunn, R. Jeffrey, Simantob, Ebrahim

13a TYPE OF REPORT	13b TIME COVERED	14 DATE OF REPORT (Year, Month, Day)	15 PAGE COUNT
Report 2 of a Series	FROM _____ TO _____	April 1989	69

16 SUPPLEMENTARY NOTATION
Available from National Technical Information Service, 5285 Port Royal Road, Springfield, VA 22161.

17 COSATI CODES			18 SUBJECT TERMS (Continue on reverse if necessary and identify by block number)
FIELD	GROUP	SUB-GROUP	Centrifuge modeling; Modeling of models; Embankment dams; Overtopping; Erosion

19 ABSTRACT (Continue on reverse if necessary and identify by block number)

An experimental program involving three rigid and three erodible model embankments is described. The rigid embankments are constructed of aluminum and are used to evaluate flow quantity and to measure resulting water velocities as well as to perform a modeling of models study.

Erodible embankment models were constructed of characteristic soils and were used to evaluate and document erosion in the scale models. Three scaling ratios used during this study were 1/24th scale, 1/49th scale, and 1/71st scale for both the rigid and erodible embankments. The system delivering overtopping water to the model is described along with other details of the centrifuge equipment and specimen preparation and testing techniques.

A total of seven tests was performed in this investigation in which erosion rates were documented and time scaling factors were determined. The study confirmed that model behavior

(Continued)

20 DISTRIBUTION/AVAILABILITY OF ABSTRACT	21 ABSTRACT SECURITY CLASSIFICATION
☒ UNCLASSIFIED/UNLIMITED ☐ SAME AS RPT ☐ DTIC USERS	Unclassified
22a NAME OF RESPONSIBLE INDIVIDUAL	22b TELEPHONE (Include Area Code) / 22c OFFICE SYMBOL

19. ABSTRACT (Continued).

duplicated field behavior at least qualitatively in that erosion, as the result of overtopping, begins at the toe of the slope of an embankment then progresses upslope and through the crest as complete breach is observed.

PREFACE

This study was conducted by the Department of Civil, Environmental, and Architectural Engineering at the University of Colorado, Boulder, under Department of Army Contract No. DACW39-83-C-0011, "Study of Embankment Performance During Overtopping and Throughflow." The contract was carried out under Work Unit #31710 entitled "Failure Mechanisms in Earth and Rock Fills under Critical Flow Conditions," of the Civil Works Investigative Studies Program, sponsored by the US Army Corps of Engineers (USACE). Mr. Richard Davidson and Mr. Ralph Beane were the USACE technical monitors.

The investigation was conducted by Drs. Hon-Yim Ko and R. Jeffrey Dunn and Mr. Ebrahim Simantob during calendar years 1983 and 1984. Dr. Y. H. Chen of Simons, Li, and Associates, Fort Collins, Colorado, provided experimental soil materials and prototype data for comparison to the model data. The report was written by Drs. Ko and Dunn and Mr. Simantob. Word processing was completed by Mrs. Kathy Van Veen and Mrs. Pat Wathen.

Mr. S. Paul Miller of the US Army Engineer Waterways Experiment Station (WES) was the Contracting Officer's representative. The work was performed under the general supervision of Mr. C. L. McAnear, Chief, Soil Mechanics Division, Geotechnical Laboratory (GL), and Dr. W. F. Marcuson III, Chief, GL.

During publication of this report LTC Jack R. Stephens, EN, was Acting Commander and Director of WES. Dr. Robert W. Whalin was Technical Director.

CONTENTS

CONVERSION FACTORS, U.S. CUSTOMARY TO METRIC (SI) UNITS OF MEASUREMENTS

U.S. Customary Units of Measurement Used in this Report can be converted to metric (SI) units as follows:

Multiply	By	To Obtain
inches	25.400	millimeters
feet	0.3048	metres
cubic feet per second	0.0283	cubic metres per second
pounds (mass)	0.4535924	kilograms
pounds (mass) per cubic foot	0.15709	kilonewtons per cubic metre

STUDY OF EMBANKMENT PERFORMANCE DURING OVERTOPPING AND THROUGHFLOW

Phase I: Rigid Model Studies

Phase II: Erodable Model Studies

PART I: INTRODUCTION

1. Overtopping of embankments and earth dams has been a major cause of failure and has also resulted in millions of dollars of damage in recent years. Data on actual overtopping events is scarce, and full scale tests to study the phenomenon are very expensive. Because gravity induced factors govern the failure mechanism, centrifgual modeling was proposed to study overtopping, and the feasibility of this method was shown in the initial phase of this study (Ko et al., 1984).

2. In the final stages of the feasibility study questions were raised regarding the appropriateness of centrifuge modeling of hydraulic phenomena such as open channel flow. Therefore, it was decided to perform additional centrifuge tests as a modeling of models study using rigid non-erodable embankment models to allow for the measurement of hydraulic parameters, notably flow quantity and velocity, in the centrifuge and to verify the scaling relations for these parameters.

3. The validity of any modeling experiments is best demonstrated by comparison with full scale prototype performance, and at the time the additional centrifuge tests were being planned, Simons, Li, and Associates (SLA) of Fort Collins, Colorado were constructing a series of full scale tests of highway embankment sections in a study of overtopping erosion for the Federal Highway Administration (FHWA). Thus it was decided to model one of the SLA test sections in the centrifuge tests in a two-phase test program. Phase I consisted of the non-erodable embankment tests, while Phase II utilized the same embankment geometry in erodable embankment models, constructed of the sandy clay soil used to construct the SLA embankments, and provided data on erosion rates for comparison to prototype data.

PART II: EQUIPMENT AND INSTRUMENTATION

The Centrifuge

4. The 10 g-ton geotechnical centrifuge which has been in operation at the University of Colorado at Boulder since 1978 is shown schematically in Figure II-1. This centrifuge is a Genisco Model 1230-5 G accelerator with a rebuilt symmetrical rotor to carry swinging baskets at the ends. The radius to hinges where the baskets are attached is 42 in. and that to the bottom of the baskets in the swung-up positions is 53.5 in. One basket carries the test payload, while the other carries the counterweights. The maximum payload size is 18 in. x 18 in. x 12 in. The rated capacity of the centrifuge is 10 g-tons, typically 100 g on a 200 lb payload.

5. The centrifuge is equipped with 56 electrical slip rings and two hydraulic rotary joints which have 0.250 in. ID tubing inside the centrifuge. As these rotary joints were judged inadequate in supplying the flow rates required for the overtopping experiments in this project, an additional large capacity toroid water conveyance system was added to the centrifuge as part of the feasibility study. This system is described in the original report (Ko et al., 1984).

6. The system was modified for the tests described herein to allow for measurement of flow quantity and improved control of flow by using two shut off valves as shown in Figure II-2. Both valves 1 and 2 were opened, with the end cap closed, to direct flow to the centrifuge. Valve 1 was used for flow quantity control and thus overtopping depth, while valve 2 was fully opened. To measure flow quantities after an overtopping test, valve 2 was closed while valve 1 was untouched, and the end cap removed. The flow quantity, Q in cfs, was measured by collecting the flow in a 30 gallon tank over a time period, usually approximately 20 seconds, and weighing the collected water.

Sample Container

7. The hydraulic modeling and erosion experiments were conducted in a new sample container constructed specifically for these tests. This container is shown schematically in Figures II-3 and II-4. Due to the limited space in the centrifuge swinging basket, only a portion of the SLA embankment crest and downstream slope could be modeled in most of the tests. One erodable embankment test was completed using the full SLA embankment configuration and is described in a later section. To accommodate models of various widths used in the modeling of models study, one wall of the sample container was adjustable.

8. As in the feasibility study, the water was stored in a storage reservoir located behind the embankment section and after overtopping, the water drained through drain ports in the compartment below the support floor. The crest of each test embankment was at the same elevation. The water was transmitted from the toroid catchment through a 1.25 inch O.D. PVC pipe with a diffuser at its end, to minimize turbulence of water as it flowed over the crest. To allow observation of the flow cross section and embankment erosion, a 1.0 inch thick plexiglass plate was used as a side wall of the sample container as shown in Figure II-4. A one-half inch square grid pattern was inscribed on this plate to provide a reference for measurement of flow depth and erosion depth in the photographs taken during the tests. Various basket mounting positions in the centrifuge were examined and the one adopted for these tests is shown in Figures II-3 and II-4. Mounting the container in any other position is not desirable since the free water surface would be curved due to a divergent gravity field, hence making it difficult to read the overtopping depth. As shown in Figure II-5, placing the models parallel to the artificial gravity field creates a smaller angle, γ, of divergent accelerations compared to placing the models perpendicular to the artificial gravity field.

Camera System

9. A 35 mm SLR remote control camera equipped with a flash and self winder was used during model studies of Phases I and II. The camera recorded a cross-sectional view of the test embankment shown in the mirror. Additionally all tests were viewed in real time using the closed circuit video camera, and recorded on video tape.

Water Depth Measurement

10. In the rigid model tests, the depth of overtopping was monitored by measuring the voltage drop across two copper plates immersed in the flow. In addition the water depth was also measured in reference to the grid system inscribed on the plexiglass sidewall, both by visual observation on the video screen during the test and by post-test analysis of photographs taken in flight. The two methods were in close agreement in all tests. In the erodable model tests, only the grid system was used for depth measurements.

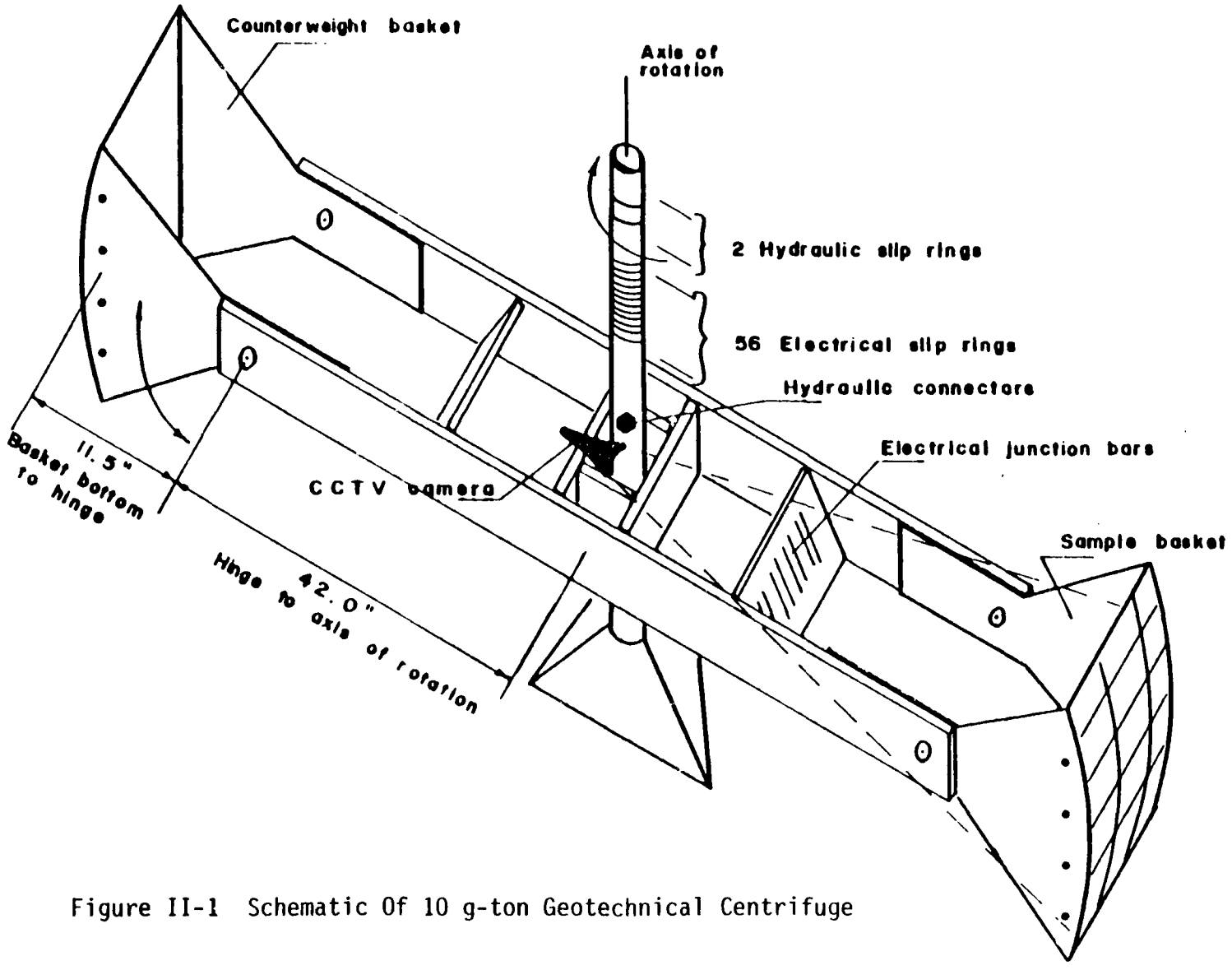

Figure II-1 Schematic Of 10 g-ton Geotechnical Centrifuge

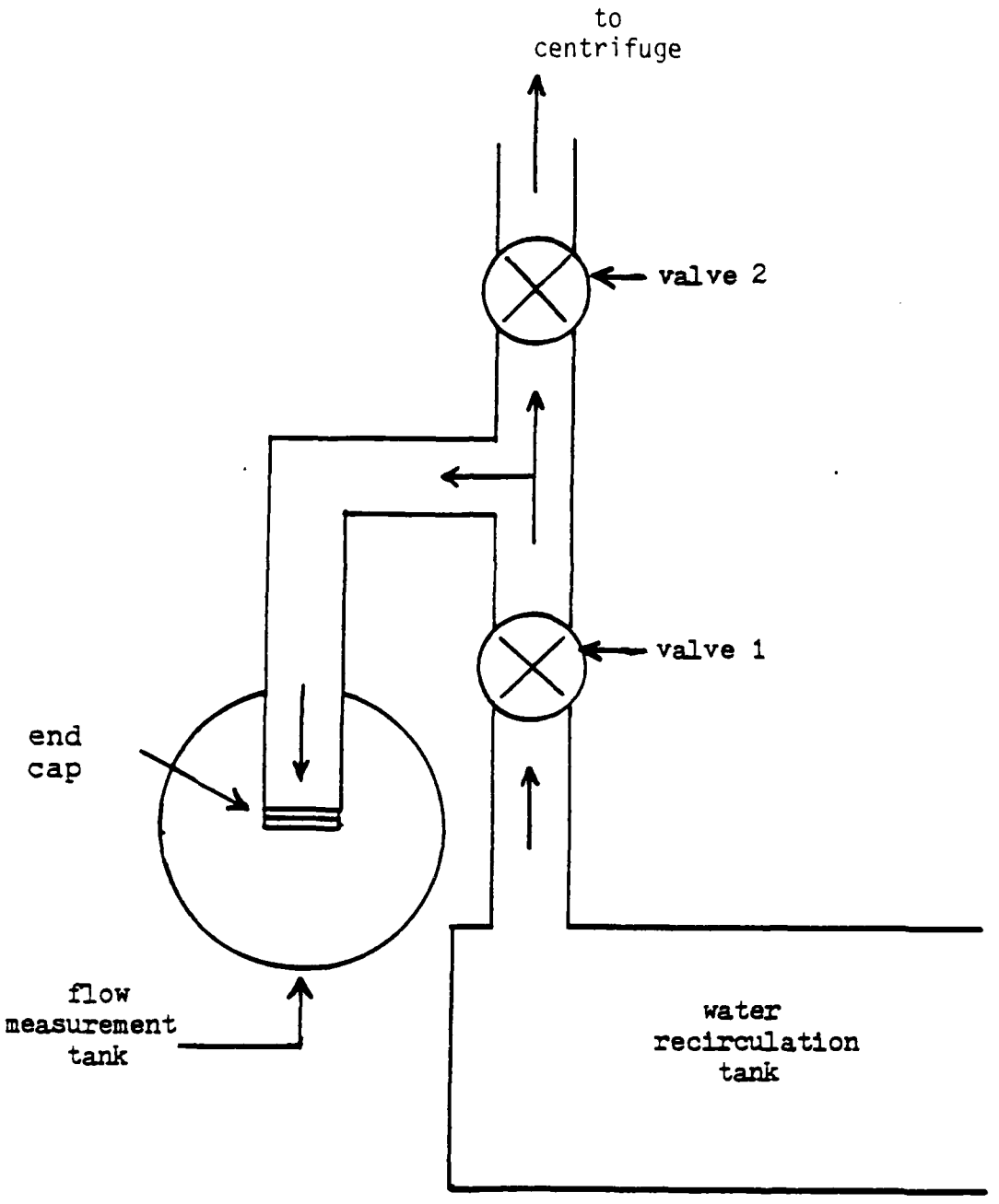

Figure II-2 Valve Arrangement For Flow Quantity Measurement

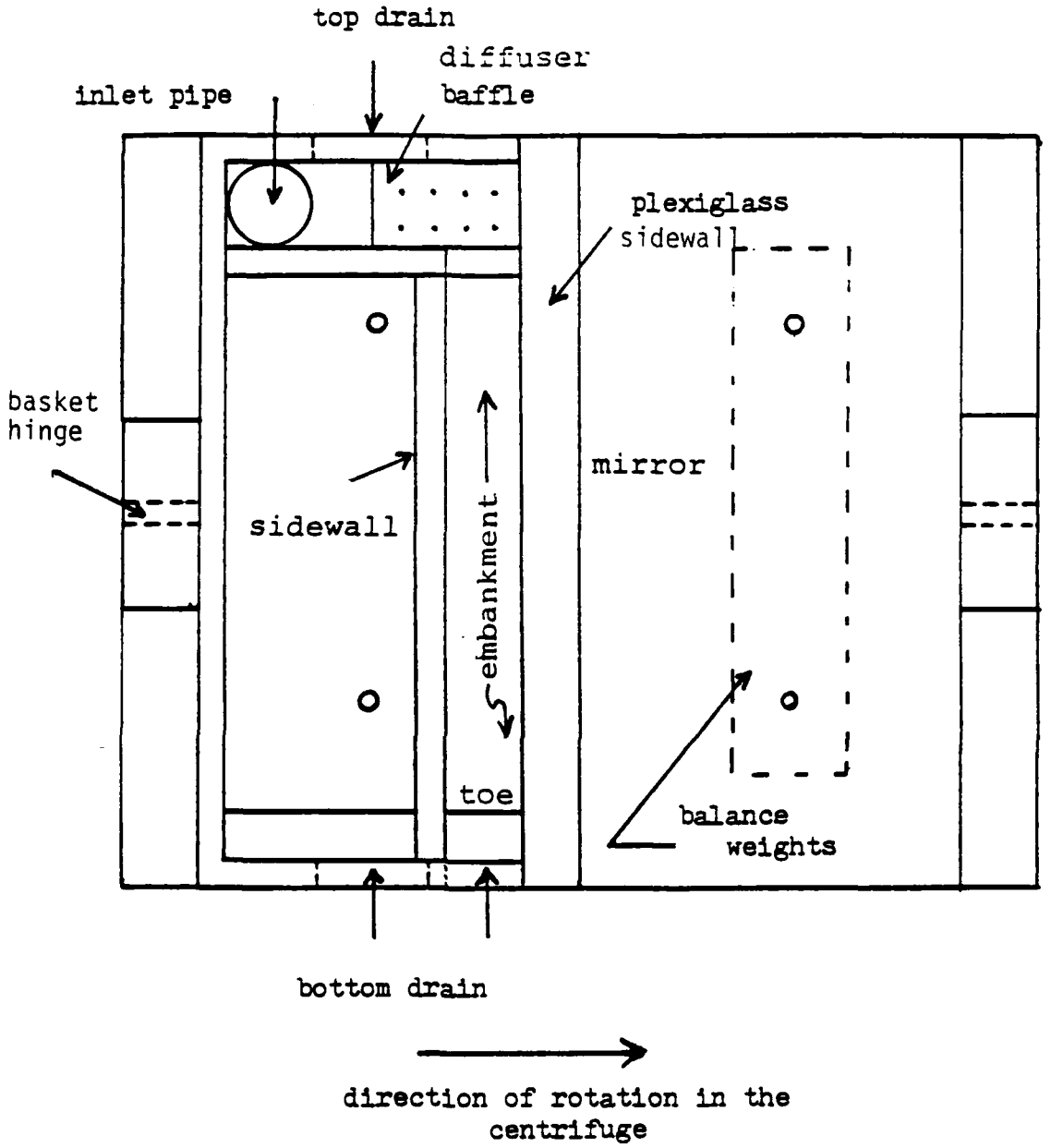

Figure II-3 Schematic Of Sample Container In Its Inflight Position, Plan View

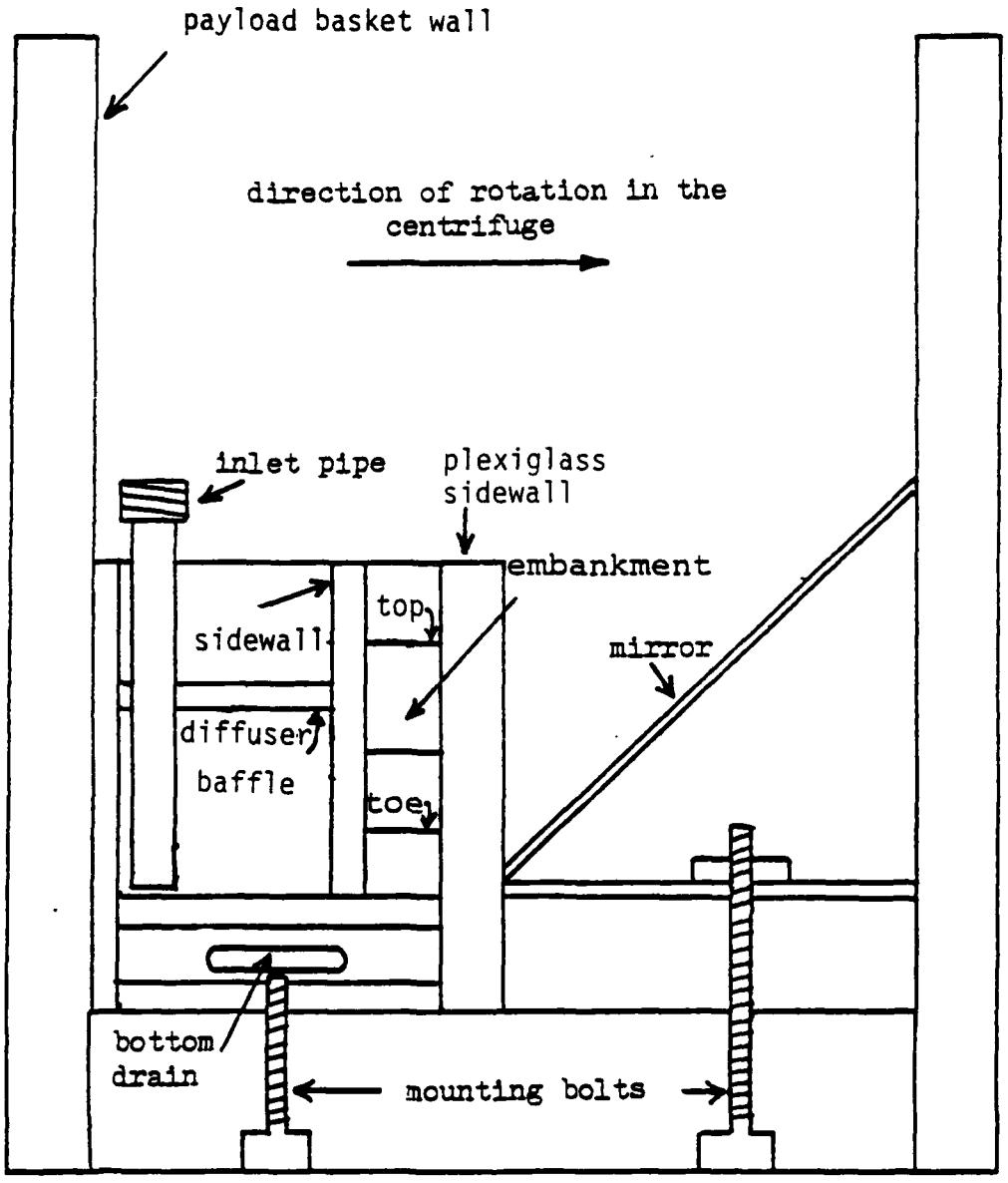

Figure II-4 Schematic Of Sample Container In Its Inflight Position, Side View

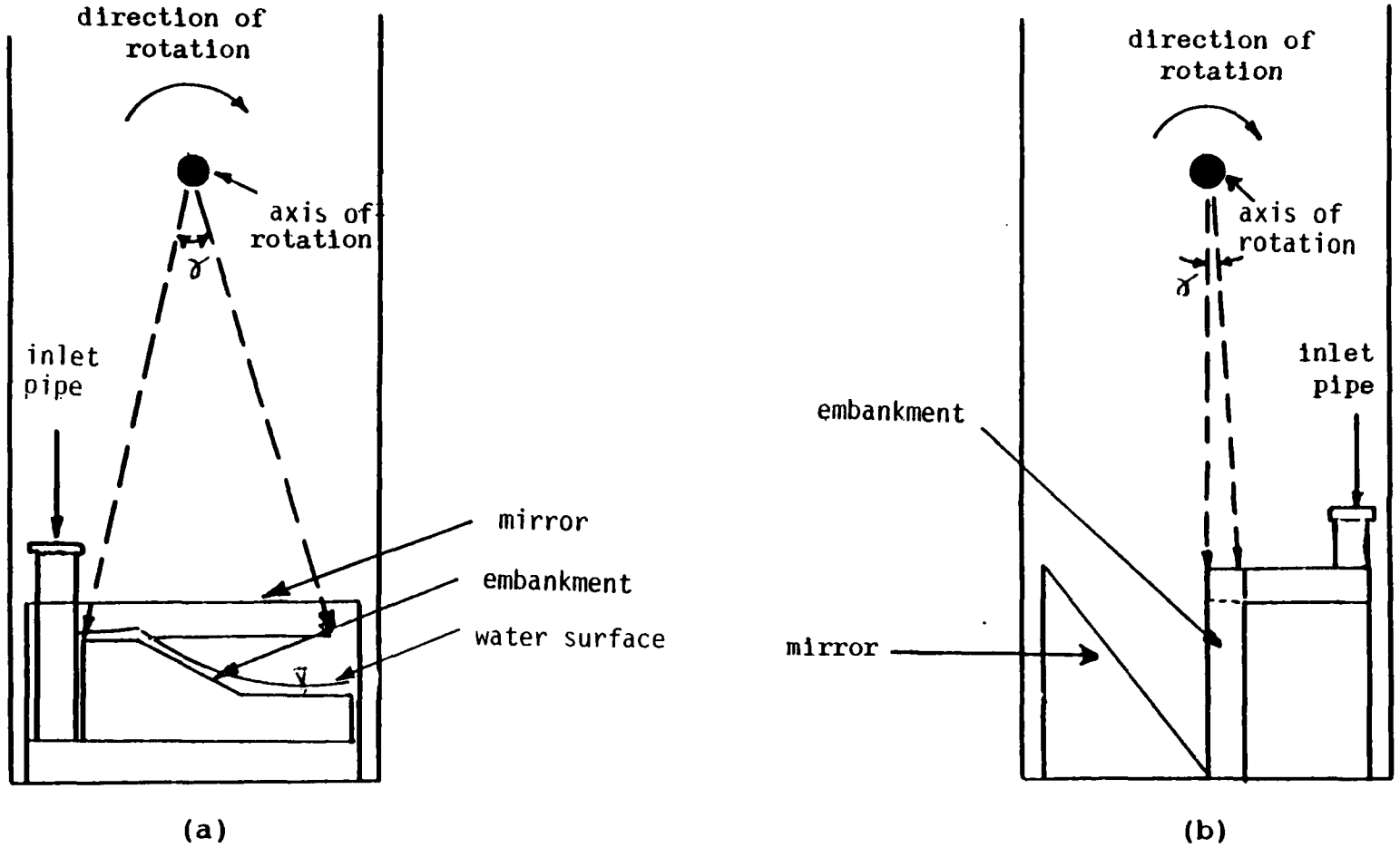

Figure II-5 (a) Initial Mounting Position Attempted
(b) Mounting Position Utilized

PART III: TEST MATERIAL AND PREPARATION OF SAMPLE EMBANKMENTS

Phase I - Rigid Embankments

11. The configuration of the prototype SLA embankment is shown in Figure III-1. This configuration was simplified so that the crest was flat rather than having the compound slope shown in the figure. Three scale models of this embankment were prepared: 1/24th, 1/49th, and 1/71st scale. When accelerated at 24, 49, and 71 g's, respectively, these models represent the prototype SLA embankment. All models were constructed of aluminum and the flow surfaces were machined using an end mill to create a smooth surface. As indicated previously due to space limitations only a portion of the crest and the downstream slope were modeled. Additionally, in the 1/24th model no toe section was modeled. The configurations of the three models are shown in Figures III-2 through III-4.

12. The front sides of the embankments were painted flat black, while the backwall of the sample container was painted pink, to provide contrast with the overtopping water which was dyed blue, thus facilitating measurement of the flow overtopping depth in the photographs.

Phase II - Erodable Embankments

Soil Material

13. The sandy clay soil used by SLA for prototype embankment construction was also used for construction of the erodable embankment models. Soil properties and the grain size curve for this material are shown in Table III-1 and Figure III-5 respectively. The grain size distribution was not scaled downward for two reasons. First, the behavior of clay soils is primarily dependent on surface forces, rather than gravity induced body forces, due to their small particle size. Second, scaling of the grain size distribution would require an elaborate centrifugation process to separate the soil grains for reconstitution.

Preparation of the Test Embankments

14. The soil obtained from the field was oven dried at 110°C, and crushed in a mechanical crusher and passed through a No. 8 sieve to eliminate any large clods or pieces of gravel. Sufficient dry material to form a single embankment was mixed in an electric mixer with the appropriate quantity of water to obtain an optimum water content of 14%. The material was then compacted statically using a hydraulic press by the undercompaction method (Ladd, 1978) in 0.5 inch layers in the sample container to a dry density of 106 pcf (90% of Modified Poctor Maximum Dry Density) at a moisture content of 14% into a rectangular block as shown in Figure III-6. The surface of each layer was thoroughly scarified prior to placing the subsequent layers. Density was verified by weighing the sample container after completion of compaction. Following the compaction, the plexiglass front wall was removed and the embankment configuration was trimmed using a sharp knife and template to the same configuration used in the three rigid embankments shown in Figures III-2 through III-4. In addition to the models with the same geometry as the rigid embankments, one additional test was performed to model the entire geometry of the full scale SLA test at 1/71st scale. The single 1/71st scale test embankment constructed with upstream and downstream slopes is shown in Figure III-7.

15. The sample container backwall was painted pink as in the case of the rigid embankments, in order to provide contrast with the blue overtopping water and brown soil.

16. The compaction procedure used for embankment preparation was different than that used by SLA for the actual embankment sections. According to information obtained from SLA the field embankments were compacted directly in the test flume. The material was compacted at a moisture content of 18% in 6 inch thick lifts using a manual jumping jack type compactor to 95% of Standard Proctor Maximum Dry Density. Thus while model and prototype densities were comparable, compaction varied in lift thickness, moisture content, and compaction method.

TABLE III-1

PROPERTIES OF SANDY CLAY TEST SOIL

UNIFIED SOIL CLASSIFICATION	CL/ML & OL
GRAIN SIZE DISTRIBUTION	
(100% passing #4)	
Percent Sand (+ #200)	37
Percent Silt	50
Percent Clay (-2μm)	13
ATTERBERG LIMITS	
Liquid Limit	39
Plastic Limit	26
Plasticity Index	13
COMPACTION PROPERTIES	
(Modified Proctor)	
Maximum Dry Density	118 pcf
Optimum Water Content	14%

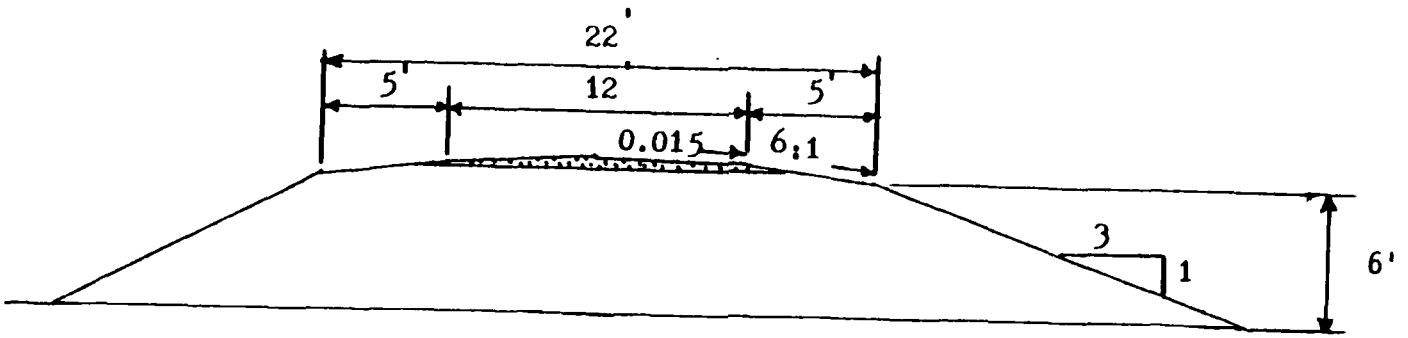

Figure III-1 SLA Prototype Test Embankment Configuration

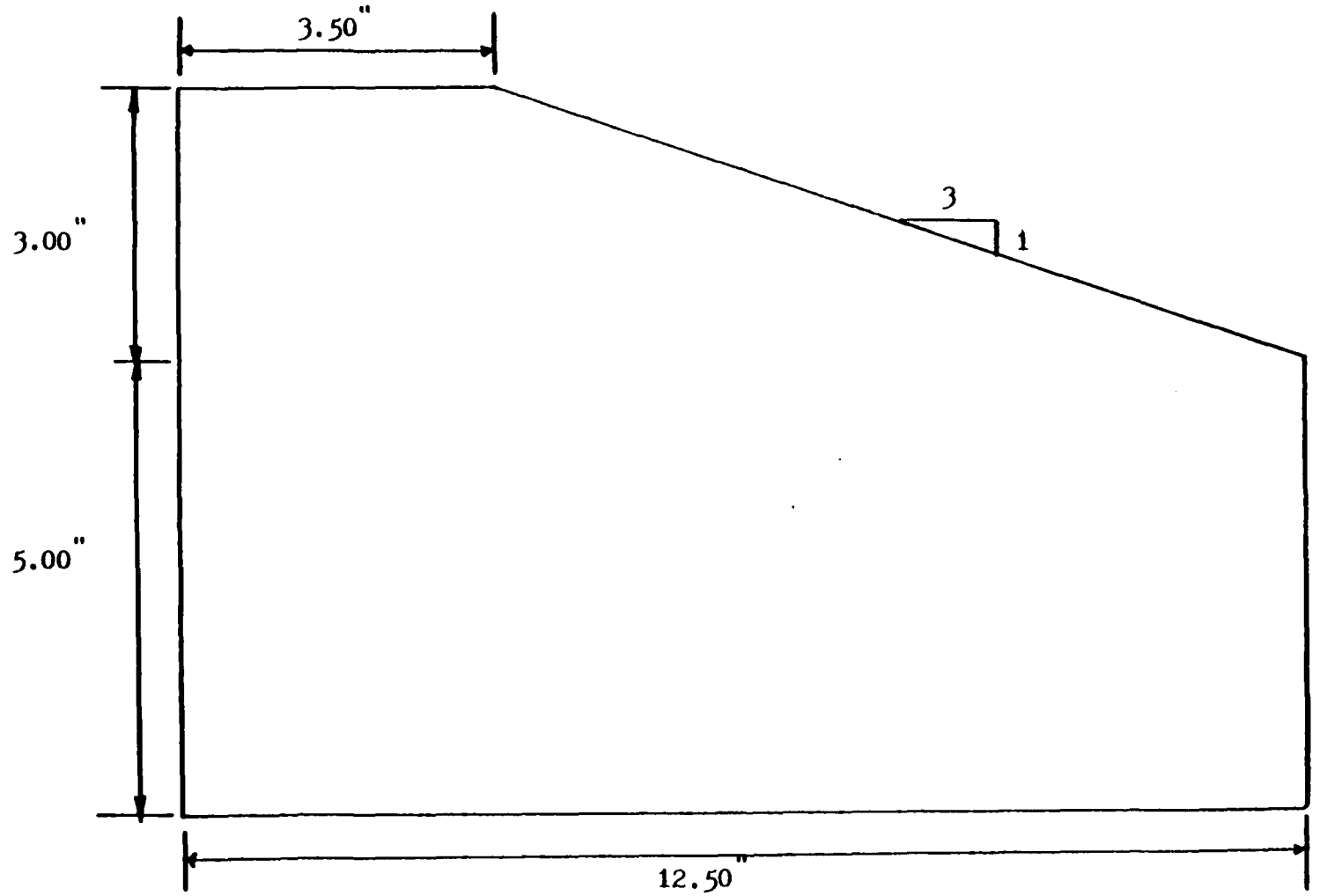

Figure III-2 1/24th Scale Rigid Embankment, 1.50" In Thickness

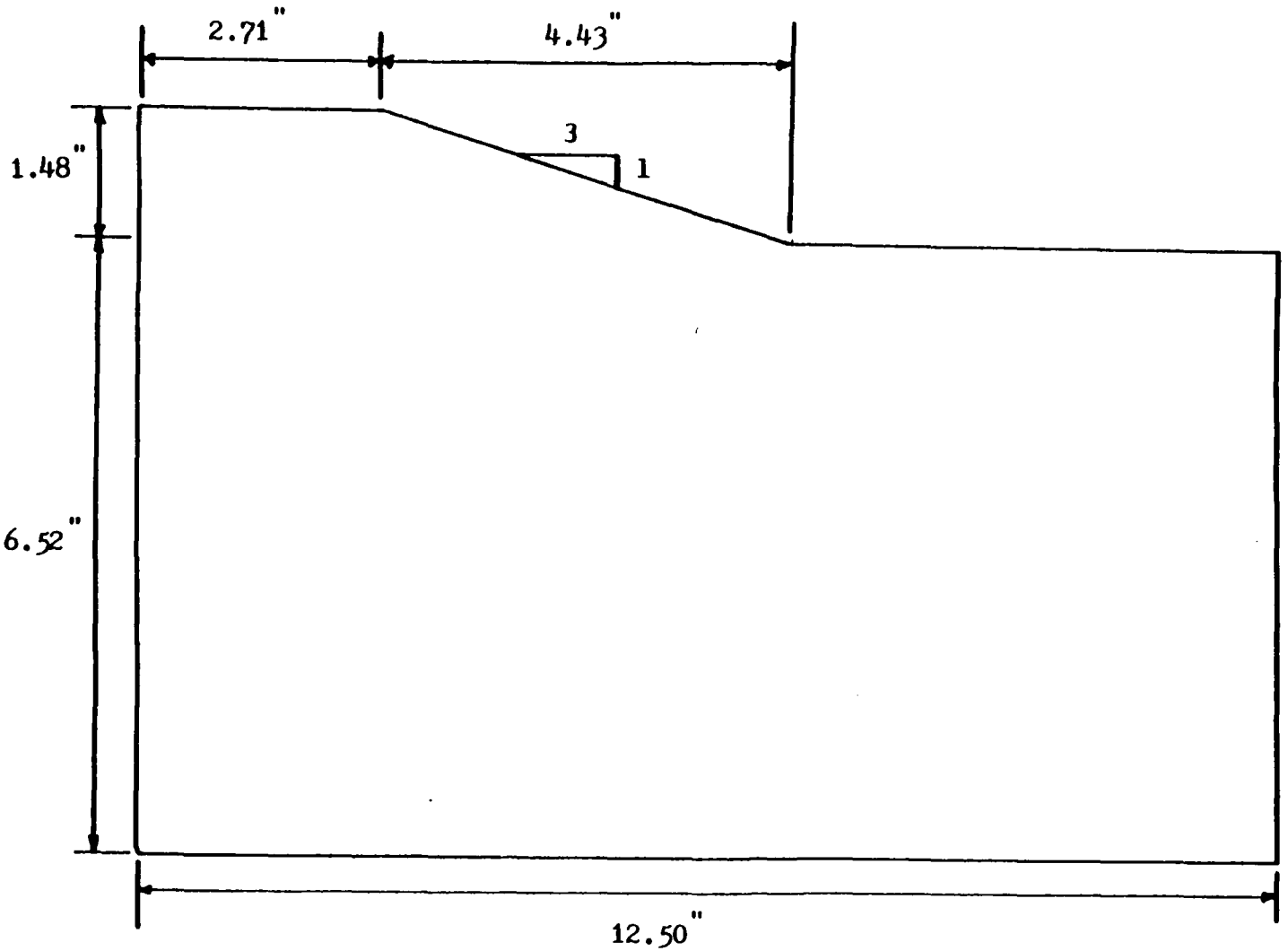

Figure III-3 1/49th Scale Rigid Embankment, 0.74" In Thickness

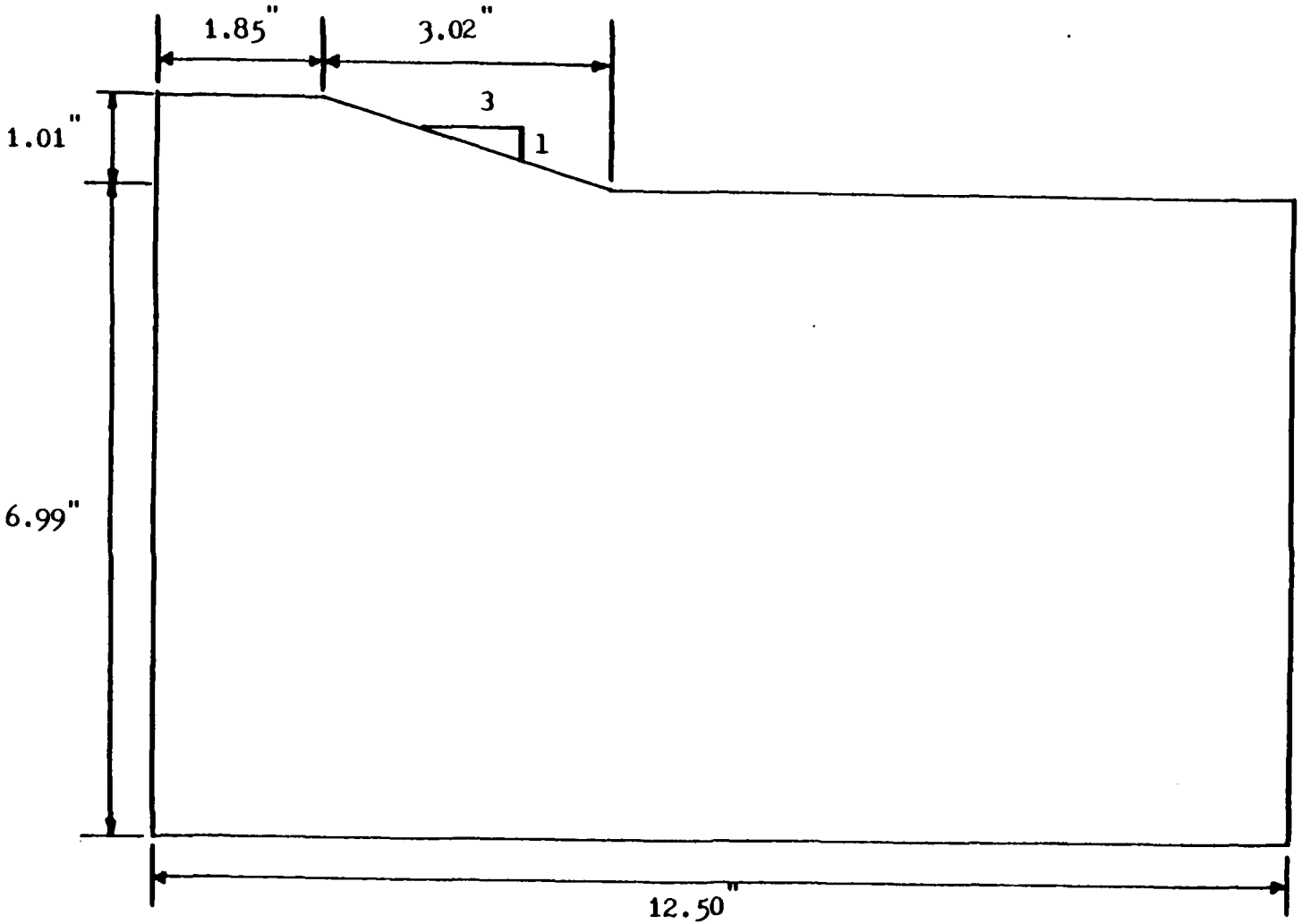

Figure III-4 1/71st Scale Rigid Embankment, 0.50" In Thickness

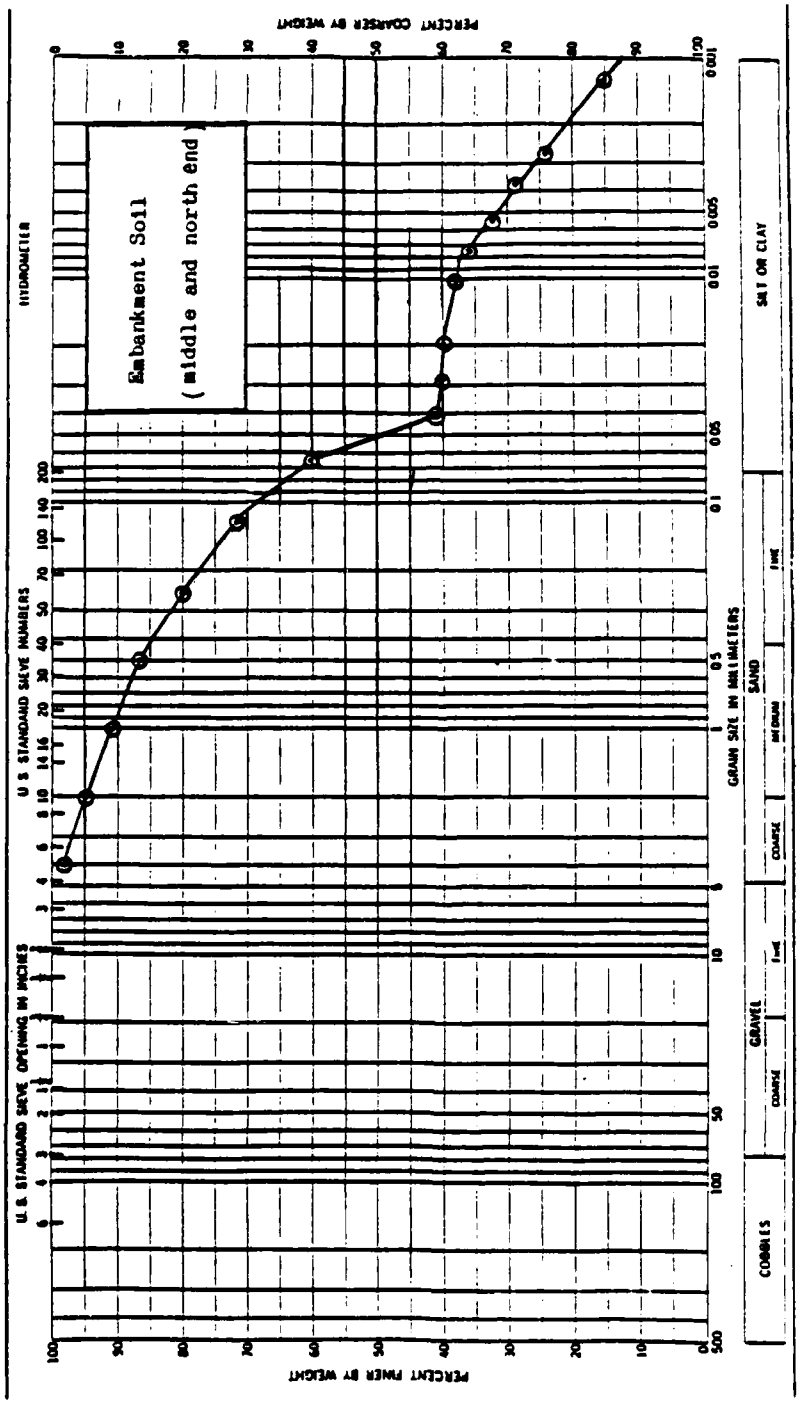

Figure III-5 SLA Embankment Soil Grain Size Distribution

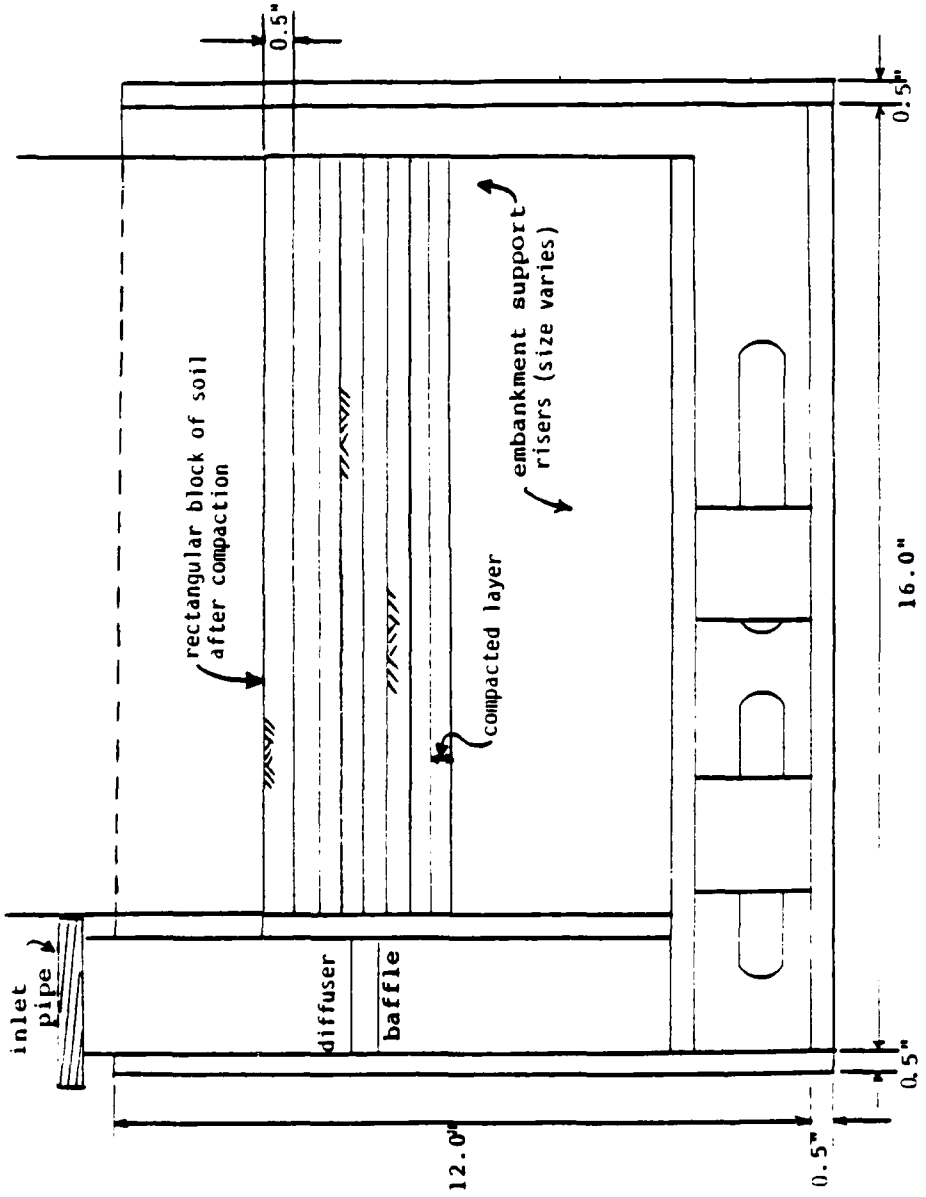

Figure III-6 Erodable Embankment Compaction Configuration

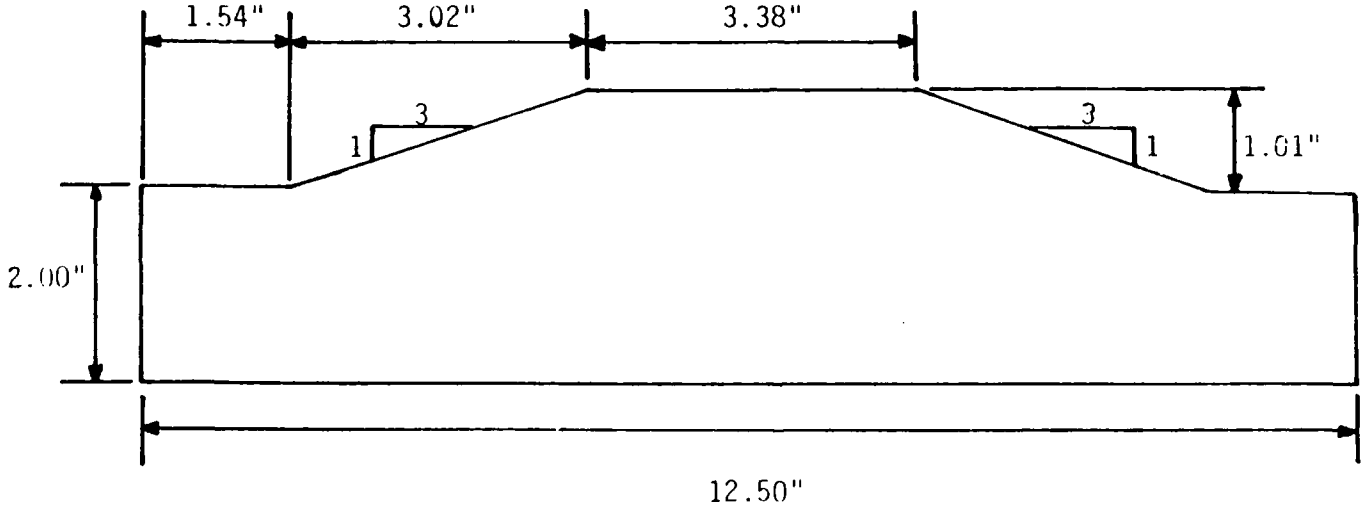

Figure III-7 1/71st Scale Erodable Full Embankment Section Model
0.50" in Thickness

PART IV: TEST PROCEDURE

Phase I - Rigid Embankment Tests

17. Three rigid embankment models were used in this segment of the study to perform a "modeling of models" study, and to evaluate modeling of flow quantities, from which flow velocities can be readily calculated. After installation of an embankment model in the test container, this assembly was placed in the centrifuge payload basket in the configuration shown in Figure II-4. One 35 mm camera with flash in combination with the video television camera was used to view the flow cross section through the mirror. After taking a picture with no overtopping water, the centrifuge was spun up to the speed necessary to produce the desired gravity level required for similarity of each model. Once at that speed the video tape recorder was turned on to record the experiments. Then the water pump was turned on to introduce water into the centrifuge. The centrifuge speed was adjusted as necessary to maintain the proper g level. The overtopping depth was determined using the electrical depth meter installed in the back compartment reservoir and the grid system inscribed on the plexiglass wall of the test container. Photos were taken by remote control, and the flow quantity was measured using the method described previously. The overtopping depth was then increased to a higher value, the centrifuge speed adjusted as necessary, photos taken, and the flow quantity measured. After sufficient measurements were taken, the water pump was turned off and the centrifuge was slowly brought to a stop.

Phase II - Erodable Embankment Tests

18. Three erodable soil embankment models were used in this study segment to evaluate erosion modeling, again using the modeling of models technique. After compaction and trimming of the embankment model, the test container was assembled and installed in the centrifuge

using the same configuration utilized in Phase I tests, Figure II-4. Both the single 35 mm camera and video camera were used for experimental recording. After taking an initial photo of the embankment prior to overtopping, the centrifuge was spun up to the proper speed for the desired gravity level, and the water pump was switched on. As quickly as possible the flow control valve was adjusted to achieve overtopping flow depths of 1.0 inch in the 1/24th, 0.49 inches in the 1/49th, and 0.34 inches in the 1/71st scale models. These depths all model a 2.0 ft. overtopping depth in the SLA prototype embankment.

19. Immediately upon reaching the desired overtopping depth, taken as zero time, a stopwatch was started. Pictures were taken during overtopping at the rate of about one per minute to allow monitoring and measurement of erosion. After overtopping was completed, the water pump was turned off, the centrifuge was slowly stopped, and the overtopping flow measured using the method described previously.

PART V: EXPERIMENTAL RESULTS

Phase I - Rigid Embankment Tests

20. In this phase of the experimental program tests on rigid non-erodable embankment models were completed to investigate, with a modeling of models analysis, the overtopping depth versus flow quantity relationship, from which flow velocity can easily be determined.

21. Overtopping depths were measured by mounting in-flight photograph negatives in slide mounts and projecting them at actual scale onto a sheet of paper. The embankment and overtopping flow cross-sections were then traced on the paper, and measurements then taken directly off these drawings. Data from the tests used in the analysis is tabulated in Table V-1, and corresponding photographs of the overtopping in the 1/24th, 1/49th, and 1/71st scale models are presented in Figures V-1, V-2, and V-3 respectively. Overtopping depths H were measured in the reservoir behind the embankment models. Flow quantities, measured by the method previously discussed, were divided in half as it was assumed that one-half the flow was directed to the counterweight basket. This adjusted value is listed as overtopping flow Q in Table V-1. The widths of the models are presented in the table. As shown in Figure V-4, overtopping flow in the back compartment had to turn 90° to enter the embankment flow section and it was observed that this led to a narrowing of the flow width similar to that described by Chow (1959) for contractions in a sharp crested weir. Therefore, the channel width was corrected to an effective width using the following equation proposed by Chow:

$$L = W - 0.1NH \qquad (V\text{-}1)$$

in which W is the actual embankment width, N is the number of contractions (taken as 1 in this study) and H is the overtopping depth. The flow intensity q (cfs/ft) was calculated by:

$$q = \frac{Q}{L} \qquad (V\text{-}2)$$

22. In order to evaluate modeling of the relationship between flow intensity q and overtopping depth H, the data were plotted logarithmically as shown in Figure V-5, and a least-squares analysis was used to fit curves to the data. The resulting curves were found to fit the general form:

$$q = a_n H^{\beta} \qquad (V\text{-}3)$$

where $\beta = 1.5$ and a_n is a coefficient related to the model gravity level. From the data shown in Figure V-5, $a_{24} = 16.0$, $a_{49} = 35.0$, $a_{71} = 44.7$. This coefficient a_n is governed by the following scaling relationship:

$$a_1 n_1^{\lambda} = a_n n^{\lambda} \qquad (V\text{-}4)$$

By rearranging terms, and recognizing that $n_1=1$ for the prototype situation,

$$a_n = a_1 n^{-\lambda} \qquad (V\text{-}5)$$

where a_1 is the prototype coefficient.

$$n = \frac{g_m}{g_p} \qquad (V\text{-}6)$$

where g_m and g_p are the model and prototype accelerations respectively. The study data indicated $\lambda = -0.97$.

23. The embankment sections tested are essentially broad-crested weirs, and in fluid mechanics flow over this type of section is usually defined as (Chow, 1959):

$$q = C_d \sqrt{2g}\, H^{3/2} \qquad (V\text{-}7)$$

which when modified for varying accelerations becomes:

$$q = C_{dn} \sqrt{2gn}\, H^{3/2} \qquad (V\text{-}8)$$

where C_{dn} is an experimentally determined coefficient of discharge dependent upon the entrance geometry of the weir and on n. All other terms are as previously defined. Comparing equations V-3 and V-8 and noting that the value of β found from the experimental data was indeed equal to that proposed by Chow (1959), we can see that

$$a_n = C_{dn} \sqrt{2gn} \tag{V-9}$$

Application of this relationship to the experimental data allowed us to calculate C_{dn} and to plot it as shown in Figure V-6, from which the following scaling relationship for C_{dn} can be developed:

$$C_{d1} n_1^{\Psi} = C_{dn} n^{\Psi} \tag{V-10}$$

and rearranging terms:

$$C_{dn} = C_{d1} n^{-\Psi} \tag{V-11}$$

where C_{d1} is the discharge coefficient value of the prototype. The model data indicated $\Psi = -0.47$ and $C_{d1} = 0.094$. If equation V-11 is substituted for C_{dn} in equation V-8 the relationship for flow then becomes:

$$q = C_{d1} \sqrt{2g}\, n^{(1/2-\Psi)} H^{3/2} \tag{V-12}$$

and substituting experimentally determined values for C_{d1} and Ψ, and for g the flow relationship was found to be:

$$q = 0.74\, n^{0.97} H^{3/2} \tag{V-13}$$

which if rounded off becomes,

$$q = 0.75\, nH^{3/2} \tag{V-14}$$

This equation was found to fit the experimental data shown in Figure V-5 very well.

Phase II - Erodable Embankment Tests

24. In the second phase of the study tests were completed on models of the SLA prototype embankments to develop data for evaluation of centrifuge modeling of erosion rates. To allow for development of scaling relationships governing erosion rates, the modeling of models technique was used in this phase in tests on 1/24th, 1/49th, and 1/71st scale models.

25. Inflight photographs of each test were taken, and one representative sequence from each size of model is presented in Figures V-7 to V-9. The photos show that in each test erosion started at the toe of the embankment slope and progressed upward toward the crest, creating a near-vertical erosion scarp. Minor surface erosion was also observed to occur away from the toe area, which is thought to be due to poor compaction layer contact and minor surface loosening of material during trimming of the embankment.

26. In order to measure the eroded soil volumes, the negative of inflight photos were projected, at full scale, on to sheets of paper, and the eroded shape was then outlined. The original non-eroded shape was also traced onto each sheet to facilitate measurements. Because the 1/24th scale embankment did not include a toe, its area at appropriate scale was traced on to drawings from the 1/49th and 1/71st scale embankments as shown in Figure V-10, to define the "erodable volume" for all tests in order to facilitate comparison of data. The eroded areas A were measured with a polar planimeter and erosion volume V was assumed to be equal to the product of erosion area A and the embankment thickness. The eroded volumes at any time of erosion were then normalized by dividing by the total "erodable" volume, to calculate percent of embankment eroded. Calculated data is tabulated in Table V-2 and plotted in Figure V-11. In the 1/49st scale tests, data from all three tests exhibit good agreement, while in the 1/24th and 1/71th scale models two tests agree well while the third test deviated. It is not known why this occurred; however, variations in compaction from test to

test are suspected. Data from the two tests that deviated, 24-2 and 71-2, were not included in development of modeling relationships for erosion. The erosion curves shown in Figure V-11 show behavior in which erosion was progressing at a fairly steady rate, then suddenly increased due to a large loss of material and then resumed at essentially the original or similar rate. For example, in test 24-1, erosion was progressing up to 16 minutes at a steady rate and in the next 2 minutes a large volume of soil eroded. After 19 minutes erosion rate resumed at level similar to that before 16 minutes. Furthermore, in all tests there seemed to be a primary erosion rate up to 4 minutes, then followed by an essentially linear segment, if any sudden loss of soil is neglected. The slope of these linear portions are defined as the erosion rates and were used for the modeling of models analysis.

27. The erosion depths at six points on the embankment were also measured at the locations indicated in Figure V-12, and were converted to prototype scale for analysis. The data from these measurements is presented in Figures V-13 through V-18. The variability of the data appears to be fairly random, which tends to indicate variations in compaction.

28. This variability also indicates that slope erosion is a process with a certain degree of randomness. The data shows that during the erosion process material is removed by both fairly steady surface erosion, and by discrete events in which large chunks of material are removed quite rapidly. The data contained in Table V-3 represent erosion rates for the model embankments.

29. The average rate for each model scale was calculated as shown in Table V-3 and the following relationship between model erosion rate $\dot{E}_m$ in % vol/min and scaling factor was obtained.

$$\dot{E}_m = 0.0077\ n^{1.38} \qquad \text{(V-15)}$$

where model erosion rate is defined as:

$$\dot{E}_m = \frac{V_{eroded}/V_{original}}{t} = \frac{V_e/V_o}{t} = \%\ \text{vol/min} \qquad \text{(V-16)}$$

The prototype erosion rate (n=1) was determined to be:

$$\dot{E}_p = 0.0077 \text{ \% vol/min} \qquad \text{(V-17)}$$

and thus the scaling relation for erosion rate was found to be:

$$\frac{\dot{E}_p}{\dot{E}_m} = \frac{0.0077\ n_p^{1.38}}{0.0077\ n^{1.38}} = n^{-1.38} \qquad \text{(V-18)}$$

Substituting equation (V-15) into equation (V-18):

$$\frac{\dot{E}_p}{\dot{E}_m} = \frac{(V_e/V_o)_p}{(V_e/V_o)_m} \cdot \frac{t_m}{t_p} = n^{-1.38} \qquad \text{(V-19)}$$

the scaling relationship for time in the erosion process can be determined from the experimental data as:

$$\frac{t_p}{t_m} = \frac{(V_e)_p}{(V_e)_m} \frac{(V_o)_m}{(V_o)_p} \cdot n^{1.38} \qquad \text{(V-20)}$$

The scaling relationship for volume is 1 to n^3 so equation (V-20) can be transformed to:

$$\frac{t_p}{t_m} = \frac{n^3}{n^3} n^{1.38} = n^{1.38} \qquad \text{(V-21)}$$

Full Embankment Section Test

30. One 1/71st model of the full embankment section being tested by SLA was modeled in the centrifuge to allow direct comparison of erosion data with the prototype data. The prototype overtopping depth used was 2.0 ft., along with a zero tailwater condition. The erosion data provided by SLA for comparison was from a test in which the total duration of overtopping was 17.5 hours. Inflight photographs of the model are shown in Figure V-19, and downstream slope cross-sections from the prototype and model for a range of overtopping times are presented in Figure V-20. Erosion of the crest was minimal in both the model and prototype. Cross-sections were reviewed to determine those for which model prototype agreement was best. As shown in Figure V-21 prototype erosion at 2.5 hours (150 min.) agreed very well with model

cross-sections at 1 and 3 minutes. Evaluation of the data to determine the scaling relationship for time yields the following relationships:

$$\frac{t_p}{t_m} = n^{1.18} \quad \text{(Model time = 1 minute)} \qquad \text{(V-22)}$$

$$\frac{t_p}{t_m} = n^{0.92} \quad \text{(Model time = 3 minutes)} \qquad \text{(V-23)}$$

Also shown in Figure V-21 are erosion cross-sections for model time of 8 minutes and prototype time of 13.5 hours. As indicated by the data, agreement is not as good as at the earlier times, although the shapes of the eroded downstream slopes are very similar. This later data indicates the following scaling relationships:

$$\frac{t_p}{t_m} = n^{1.08} \qquad \text{(V-24)}$$

31. The relationships shown in equations V-22 through V-24 do not agree with that determined in the modeling of models study indicated by equation V-21. If the scaling relation of equation V-21 is used, then the model time corresponding to 13.5 hrs (810 minutes) of prototype time is calculated to be 2.26 minutes. No data was available at 2.26 minutes; however, a profile at 2.0 minutes is shown in Figure V-21 for comparison. It can be seen that considerable differences are found. However, if variations in density and soil structure and thus soil erodability between the model and prototype occurred, this would result in errors in the determination of time scaling relationships of equations V-22 through V-24. As discussed previously while model densities were comparible to those attained in the prototype, the compaction procedures varied in lift thickness, compaction moisture content, and compaction method. These differences would likely result in variations in soil structure between the model and prototype embankments. However, the degree of this variation cannot be determined with the data available.

TABLE V-1

RIGID EMBANKMENT TESTS OVERTOPPING DATA

Model Scale Factor n	Channel Width W (ft)	Corrected Channel Width L (ft)	Overtopping Depth H (ft)	Overtopping Flow Q (cfs)	Unit Overtopping Flow q (cfs/ft)
24	.125	.118	.067	.031	.26
		.119	.058	.026	.22
		.119	.060	.027	.22
		.117	.079	.041	.35
		.116	.090	.049	.42
		.115	.098	.055	.47
49	.062	.058	.036	.014	.25
		.057	.044	.019	.32
		.056	.052	.024	.43
		.055	.061	.029	.52
		.054	.074	.038	.70
		.053	.086	.049	.92
		.052	.098	.054	1.1
71	.042	.039	.033	.011	.28
		.037	.049	.018	.48
		.035	.069	.027	.76
		.034	.078	.034	1.0
		.032	.098	.038	1.2

TABLE V-2

ERODABLE EMBANKMENT DATA

Model Scale Factor n	Test 1 Overtopping Time t (min)	Test 1 Eroded Volume V (%)	Test 2 Overtopping Time t (min)	Test 2 Eroded Volume V (%)	Test 3 Overtopping Time t (min)	Test 3 Eroded Volume V (%)
24	1.25	3.7	1.00	2.2	1.50	0.9
	2.33	6.8	2.00	5.5	2.17	1.6
	4.58	14.6	4.00	21.6	4.17	7.8
	8.75	23.0	8.00	54.6	8.00	13.7
	16.50	28.1	15.30	81.5	16.00	20.8
	19.75	48.1	23.00	88.7	26.00	26.0
	25.00	53.9			36.00	28.8
	30.00	55.4			46.00	35.2
	36.00	59.1				
49	1.00	4.5	0.83	1.5	0.83	0.9
	1.92	6.5	2.10	4.4	2.17	3.7
	4.17	7.9	4.08	5.6	4.17	8.2
	8.17	9.9	8.00	9.3	8.00	33.2
	17.17	12.4	16.83	11.0	11.75	38.7
	24.17	47.4	24.33	19.6	17.33	40.3
	30.17	47.8	30.50	25.8		
71	1.00	4.9	1.00	0.8	1.00	9.9
	2.00	4.9	2.00	4.8	2.00	11.9
	4.00	6.5	4.00	5.9	4.00	15.9
	8.50	28.3	8.50	26.2	8.00	32.9
	16.00	44.0	11.00	48.1	13.00	47.1
	19.00	49.2	13.00	68.1	16.00	49.5
			15.50	74.5		

TABLE V-3

EROSION RATE DATA

Model Scale Factor n	Time Range ΔT (min)	Erosion Rate $\dot{E}$ (%vol/min)	Average Erosion Rate E_{ave} (%vol/min)
24	19.75-36.00	0.64	0.62
	4.17-36.00	0.60	
49	4.17-30.17	1.74	1.57
	4.08-30.50	0.73	
	4.17-17.33	2.24	
71	4.00-19.00	2.73	2.79
	4.00-16.00	2.85	

(a)

(b)

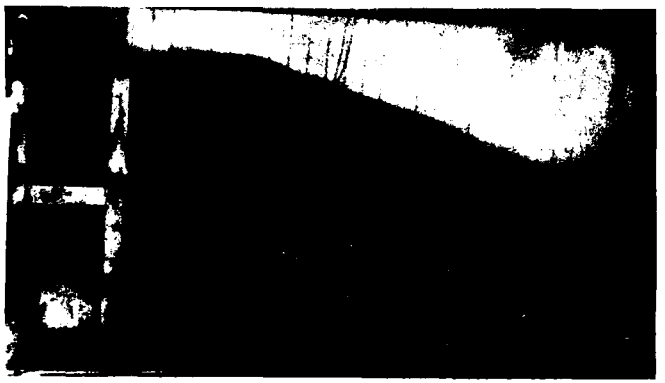

(c)

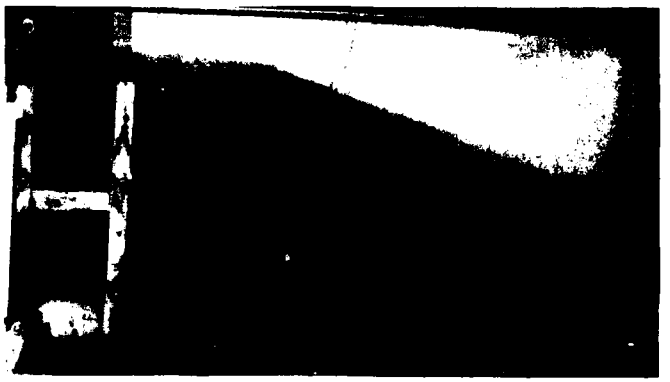

(d)

Figure V-1 1/24th Scale Rigid Embankment, (a) H=0', (b) H=0.058', (c) H=0.060', (d) H=0.067'

(e)

(f)

(g)

Figure V-1 1/24 Scale Rigid Embankment, (e) H=0.079', (f) H=0.090', (g) H=0.098'

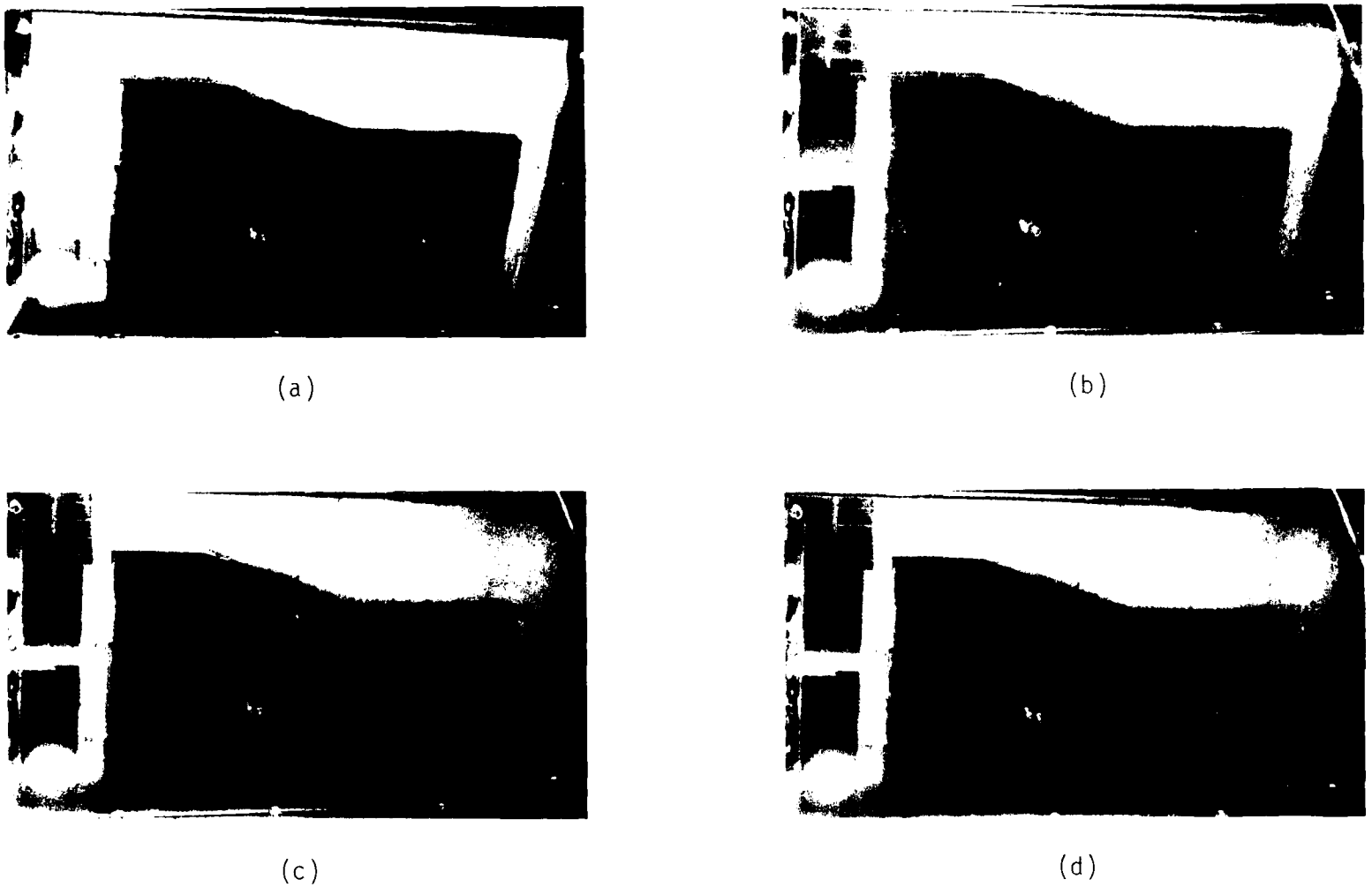

Figure V-2 1/49th Scale Rigid Embankment, (a) H=0', (b) H=0.036', (c) H=0.044', (d) H=0.052'

(e)

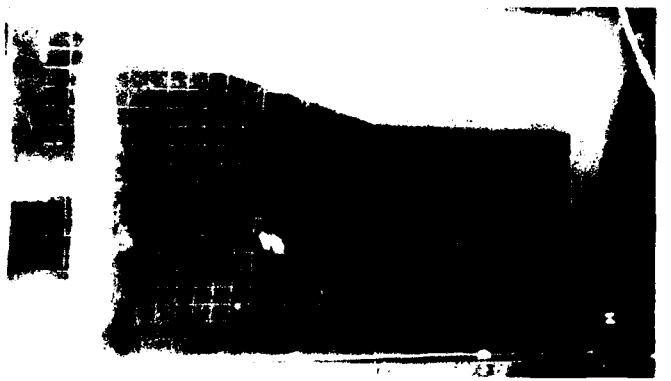

(f)

(g)

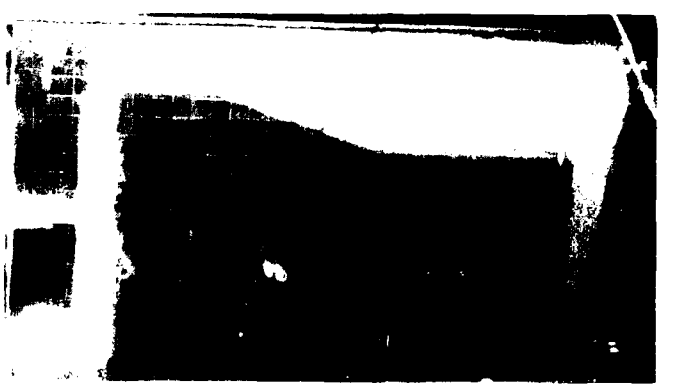

(h)

Figure V-2 1/49th Scale Rigid Embankment, (e) H=0.061', (f) H=0.074', (g) H=0.086', (h) H=0.098'

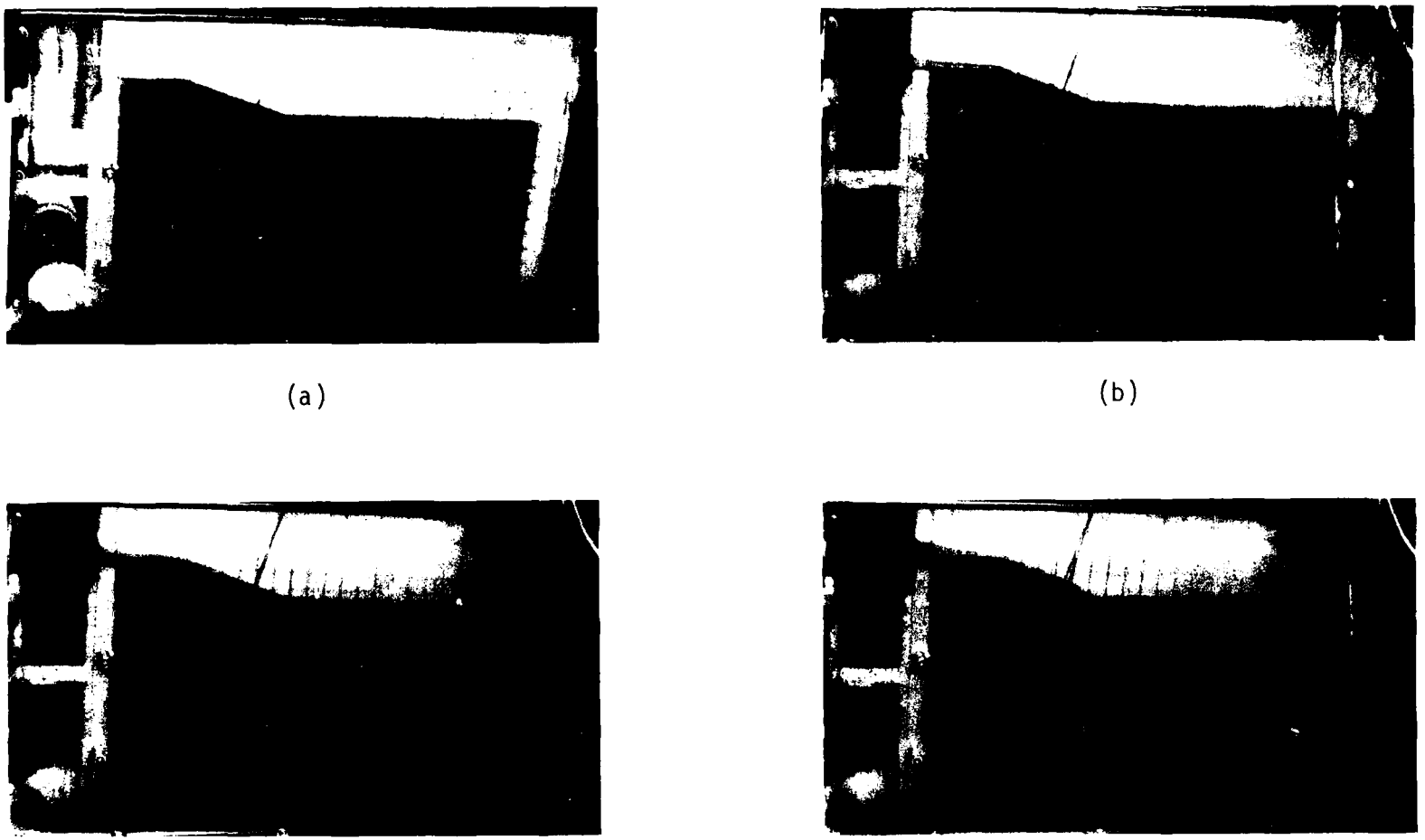

(a) (b)

(c) (d)

Figure V-3 1/71st Scale Rigid Embankment, (a) H=0', (b) H=0.033', (c) H=0.049', (d) H=0.069'

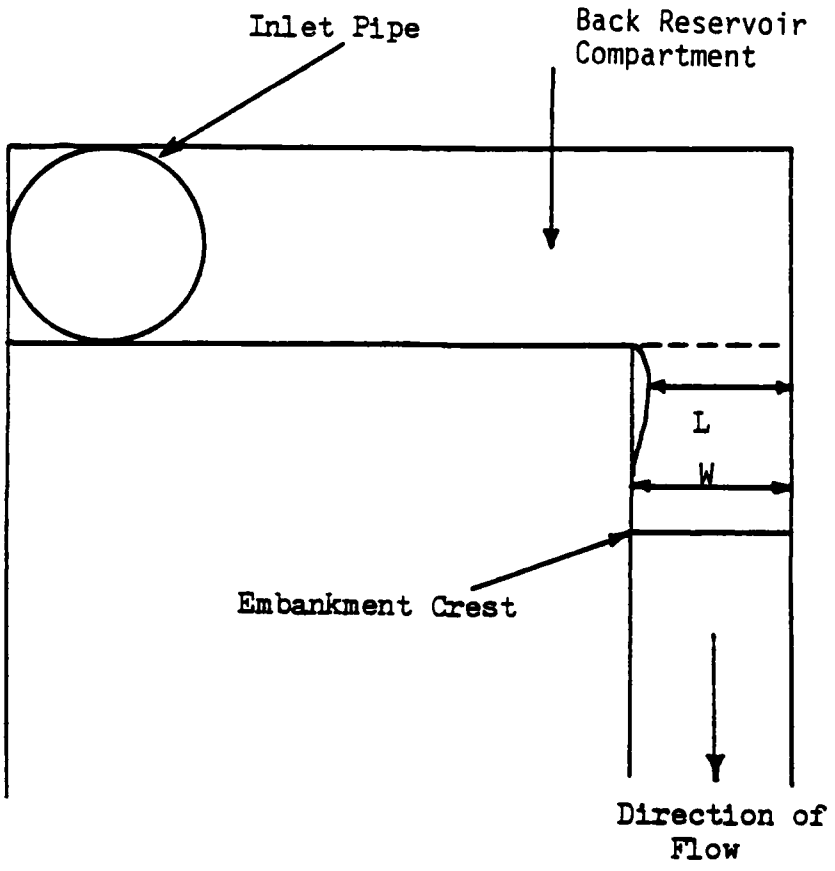

Figure V-4 Contraction Of Flow At Entrance To Embankment

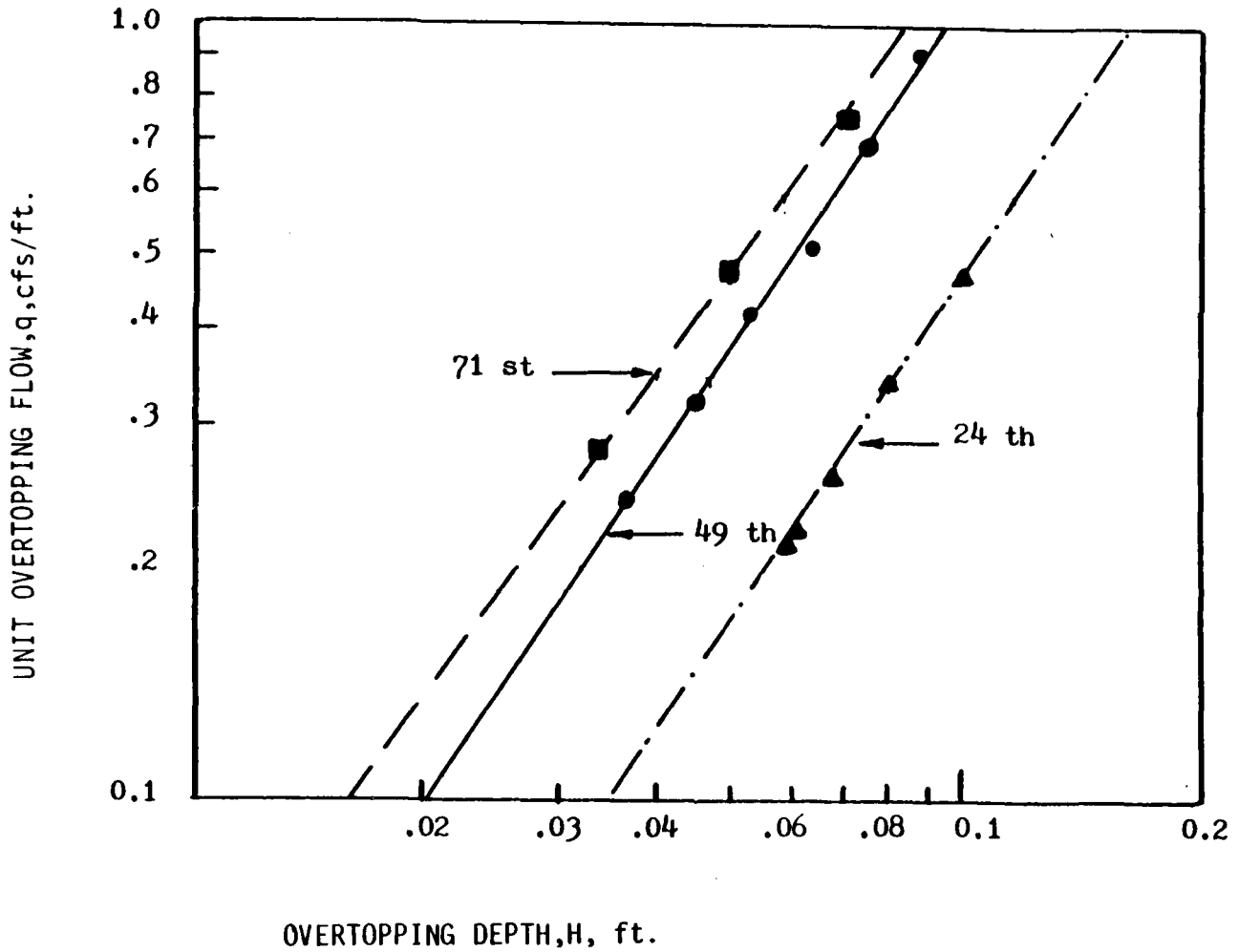

Figure V-5 Unit Overtopping Flow Versus Overtopping Depth

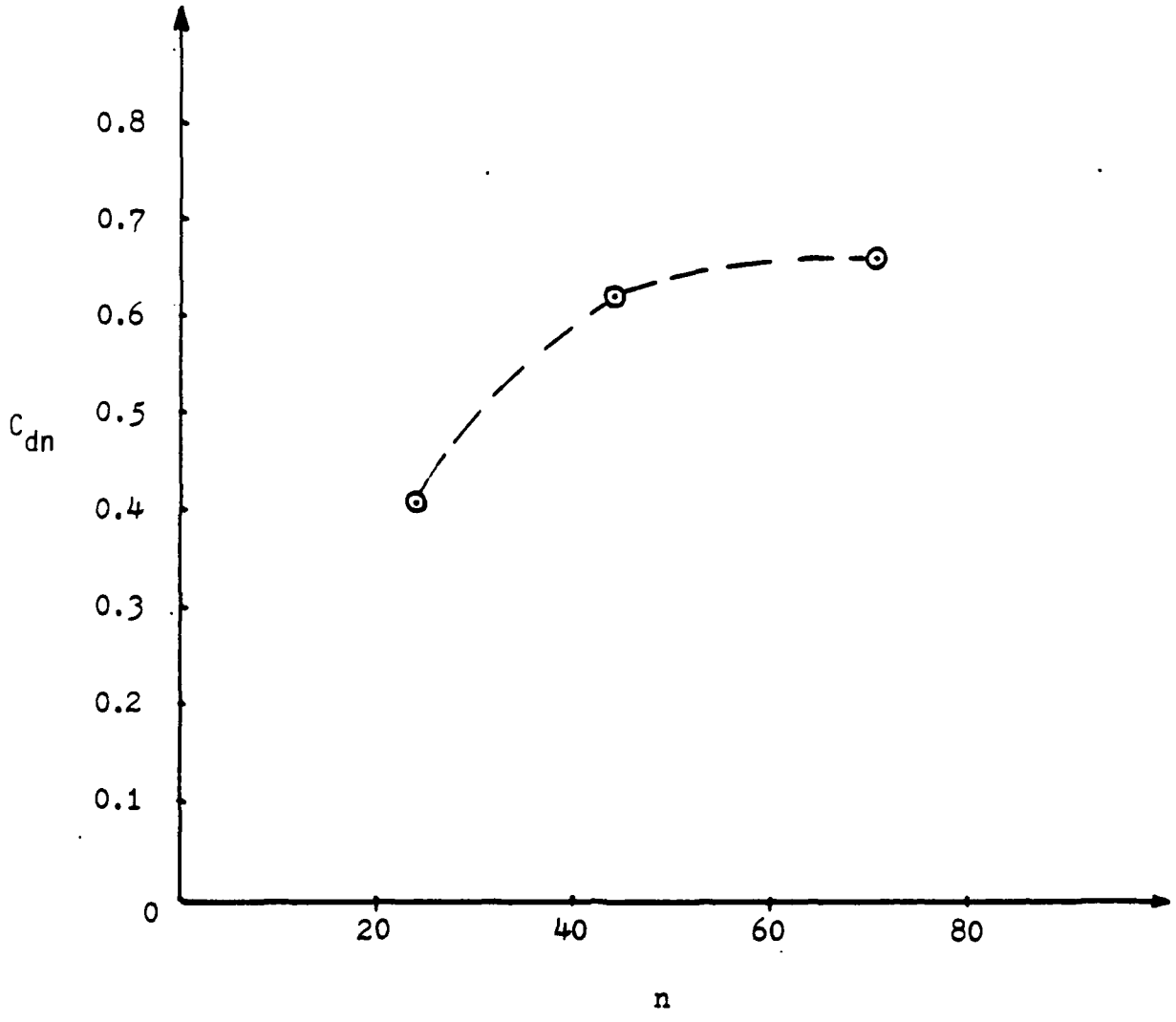

Figure V-6 Discharge Coefficient- C_{dn} Versus Model Scale Factor- n

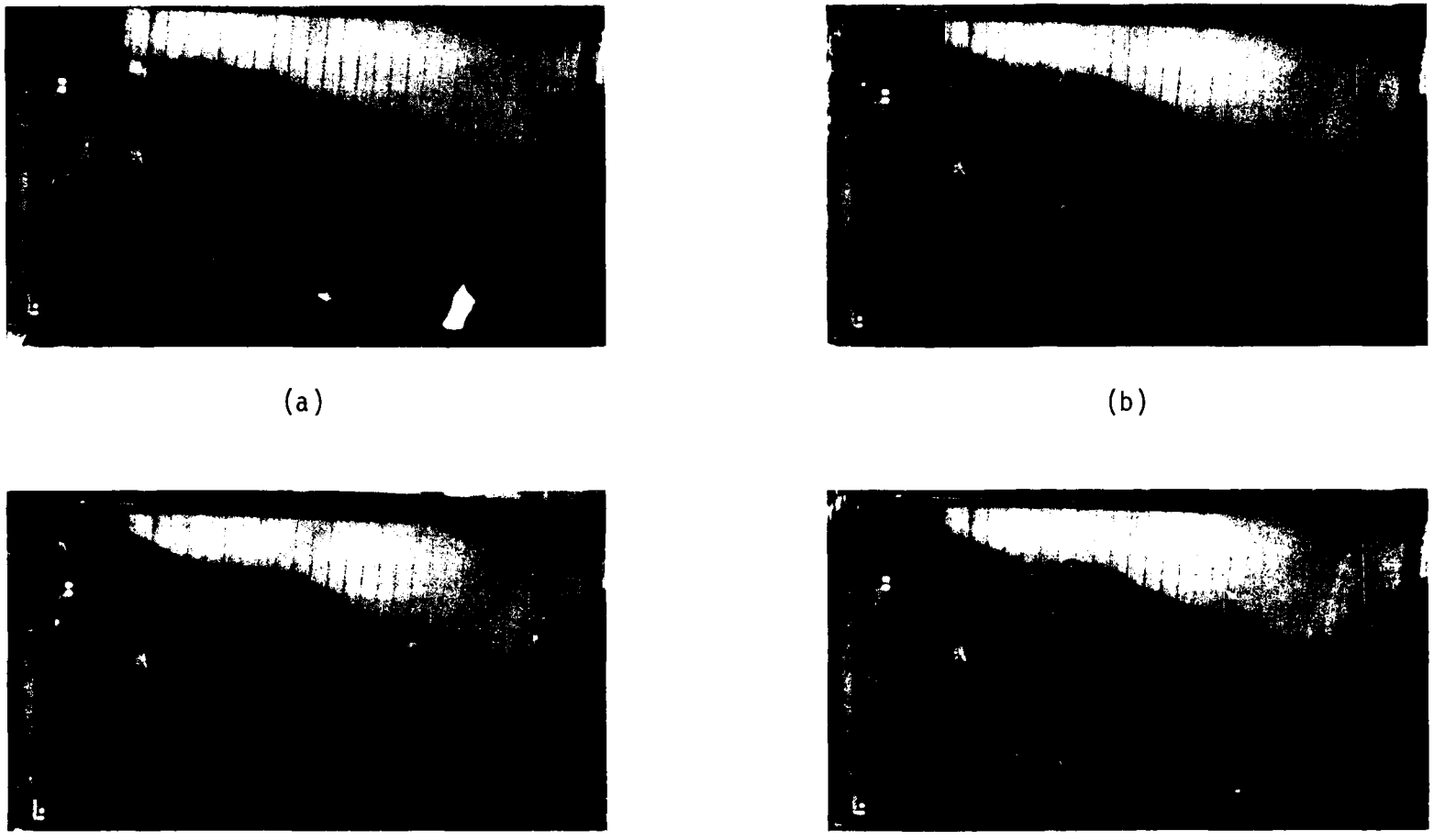

(a) (b)

(c) (d)

Figure V-7 1/24th Scale Erodable Embankment, (a) t=0 min, (b) t=1.25 min, (c) t=2.33 min, (d) t=4.58 min

(e)

(f)

(g)

(h)

Figure V-7 1/24th Scale Erodable Embankment, (e) t=8.75 min, (f) t=16.5 min, (g) t=19.75, (h) t=25 min

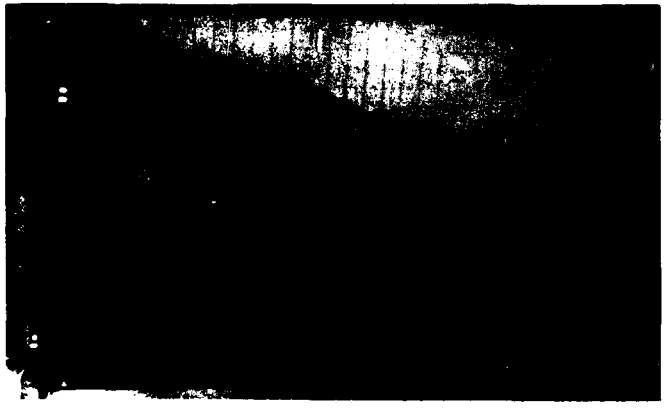

(i)

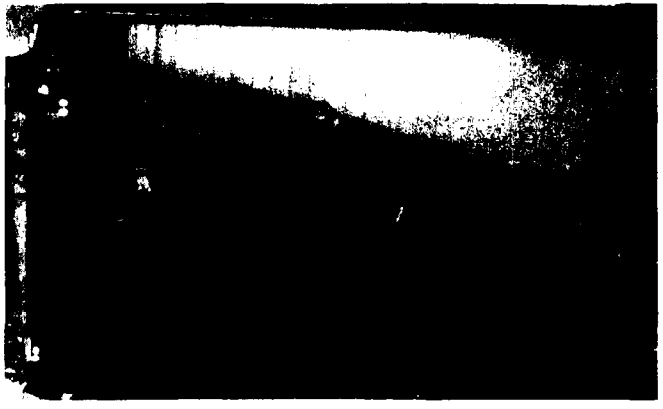

(j)

Figure V-7 1/24th Scale Erodable Embankment, (i) t=30 min, (j) t=36 min

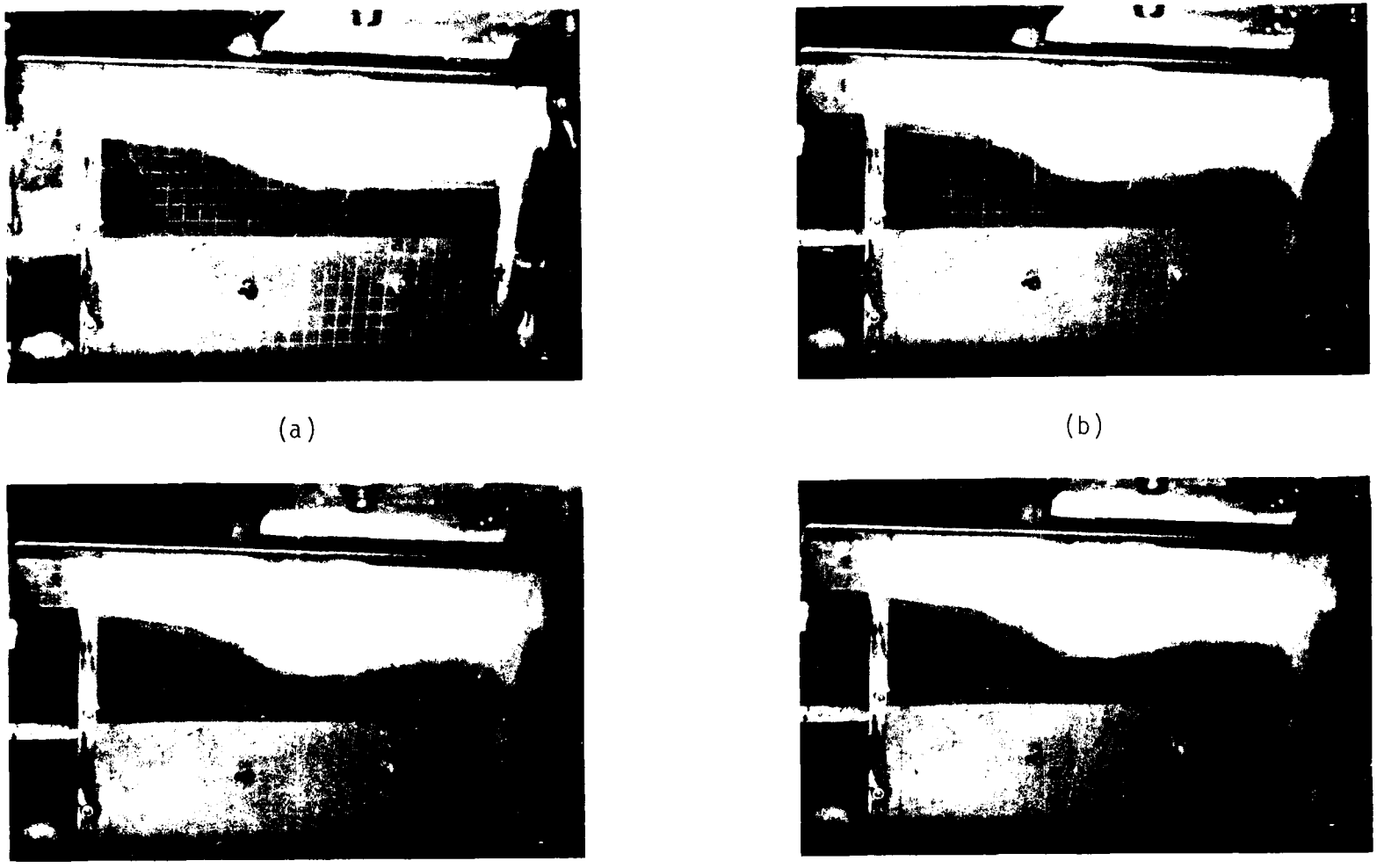

Figure V-8 1/49th Scale Erodable Embankment, (a) t=0 min, (b) t=1.00 min, (c) t=1.92 min, (d) t=4.17 min

(e)

(f)

(g)

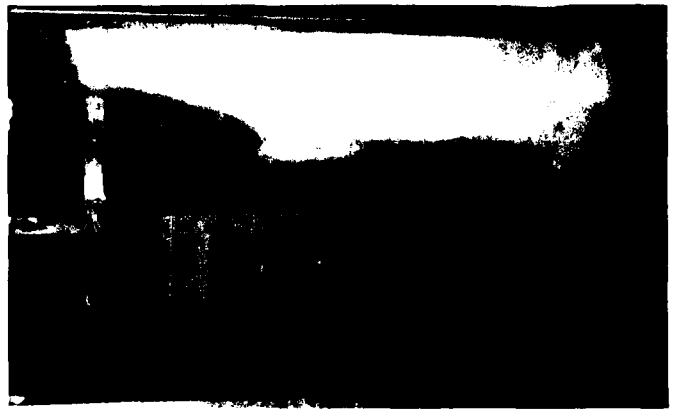

(h)

Figure V-8 1/49th Scale Erodable Embankment, (e) t=8.17 min, (f) t=17.17 min, (g) t=24.17 min, (h) t=30.17 min

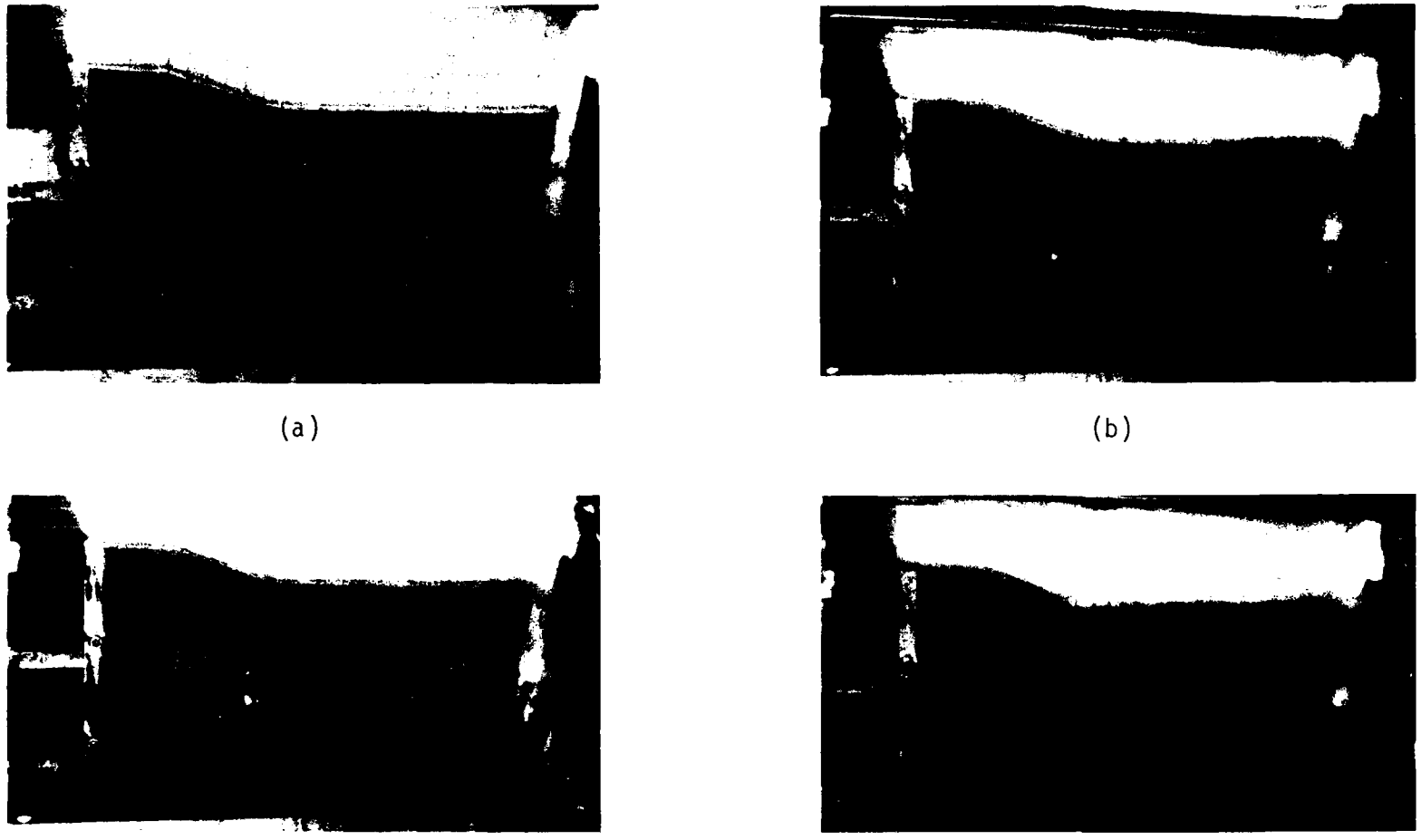

(a) (b)

(c) (d)

Figure V-9 1/71st Scale Erodable Embankment, (a) t=0 min, (b) t=1.00 min, (c) t=2.00 min, (d) t=4.00 min

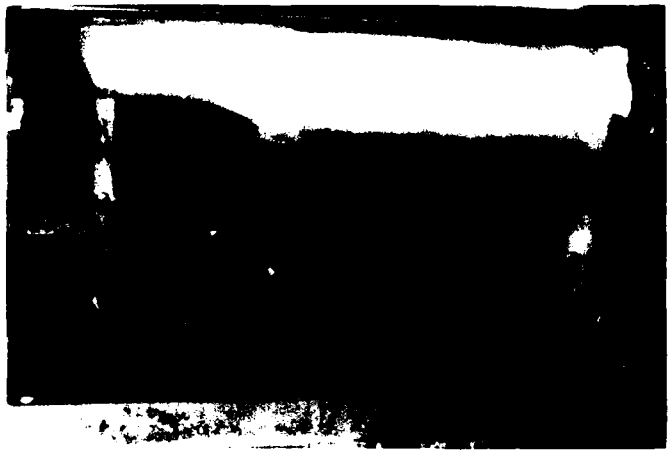

(e)

(f)

(g)

Figure V-9 1/71st Scale Erodable Embankment, (e) t=8.50 min, (f) t=16.00 min, (g) t=19.00 min

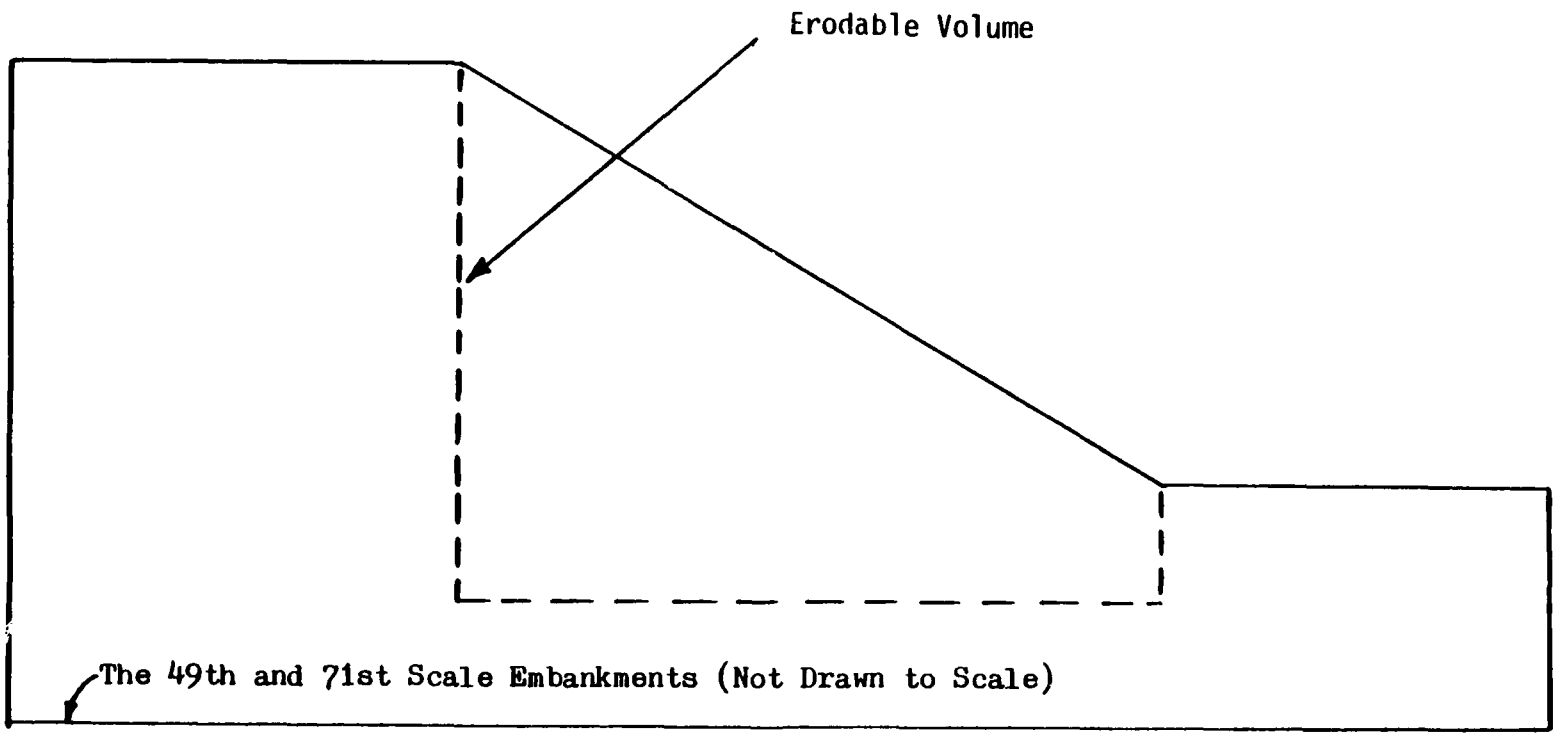

Figure V-10 Erodable Volume From 1/24th Scale Embankment Superimposed On 1/49th And 1/71st Scale Embankment Cross-Sections.

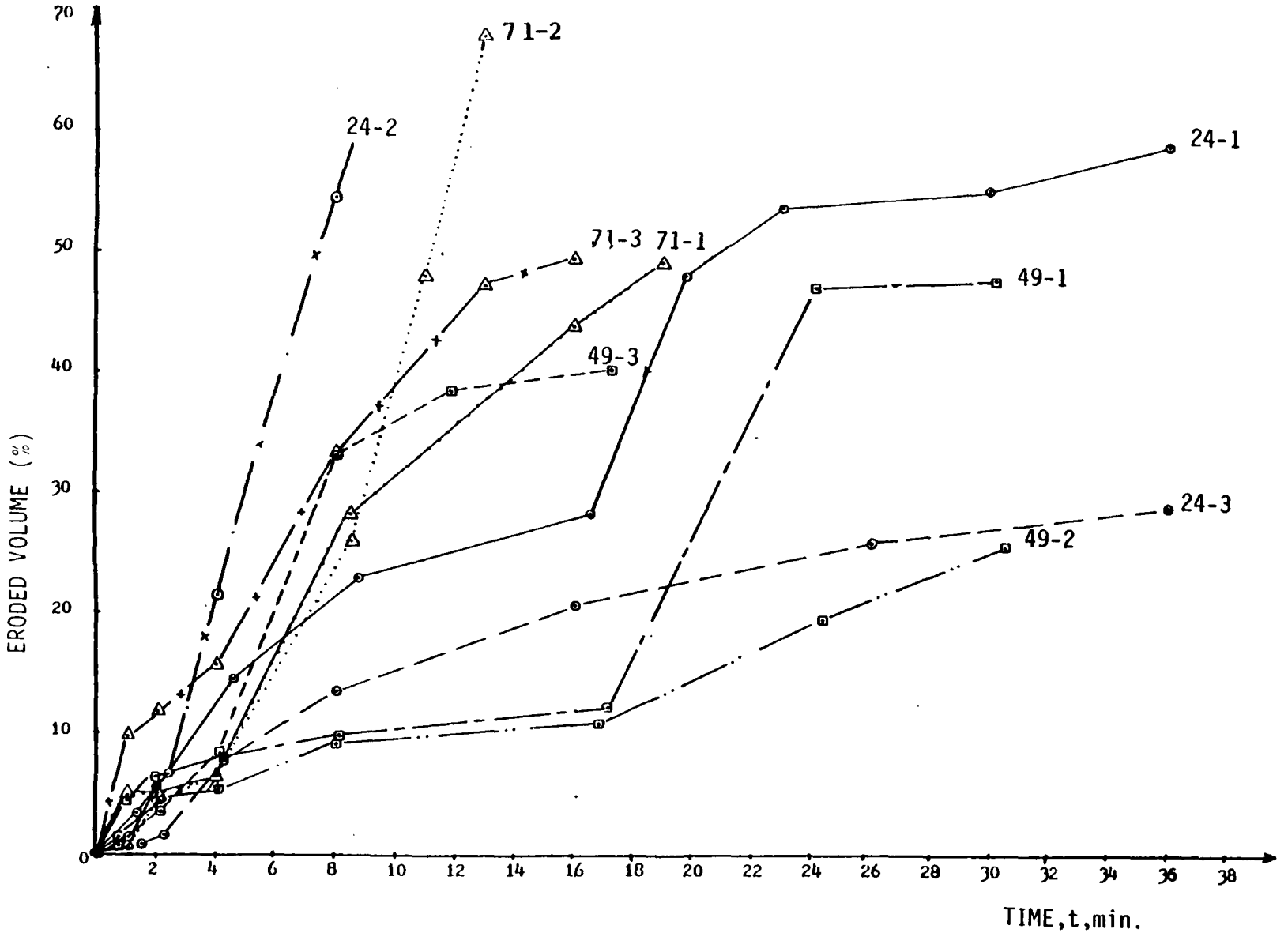

Figure V-11 Eroded Volume Versus Time

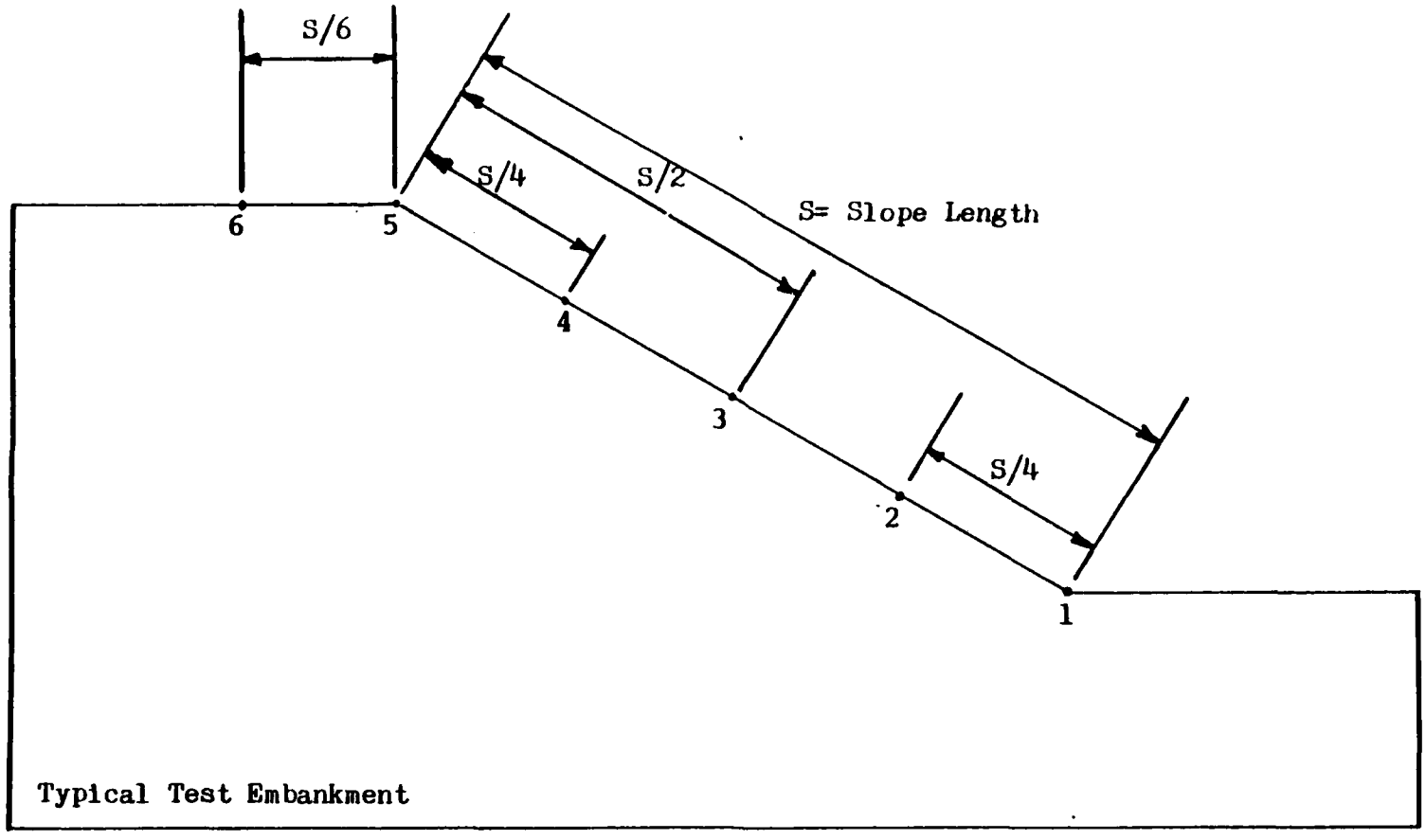

Figure V-12 Erosion Depth Measurement Locations

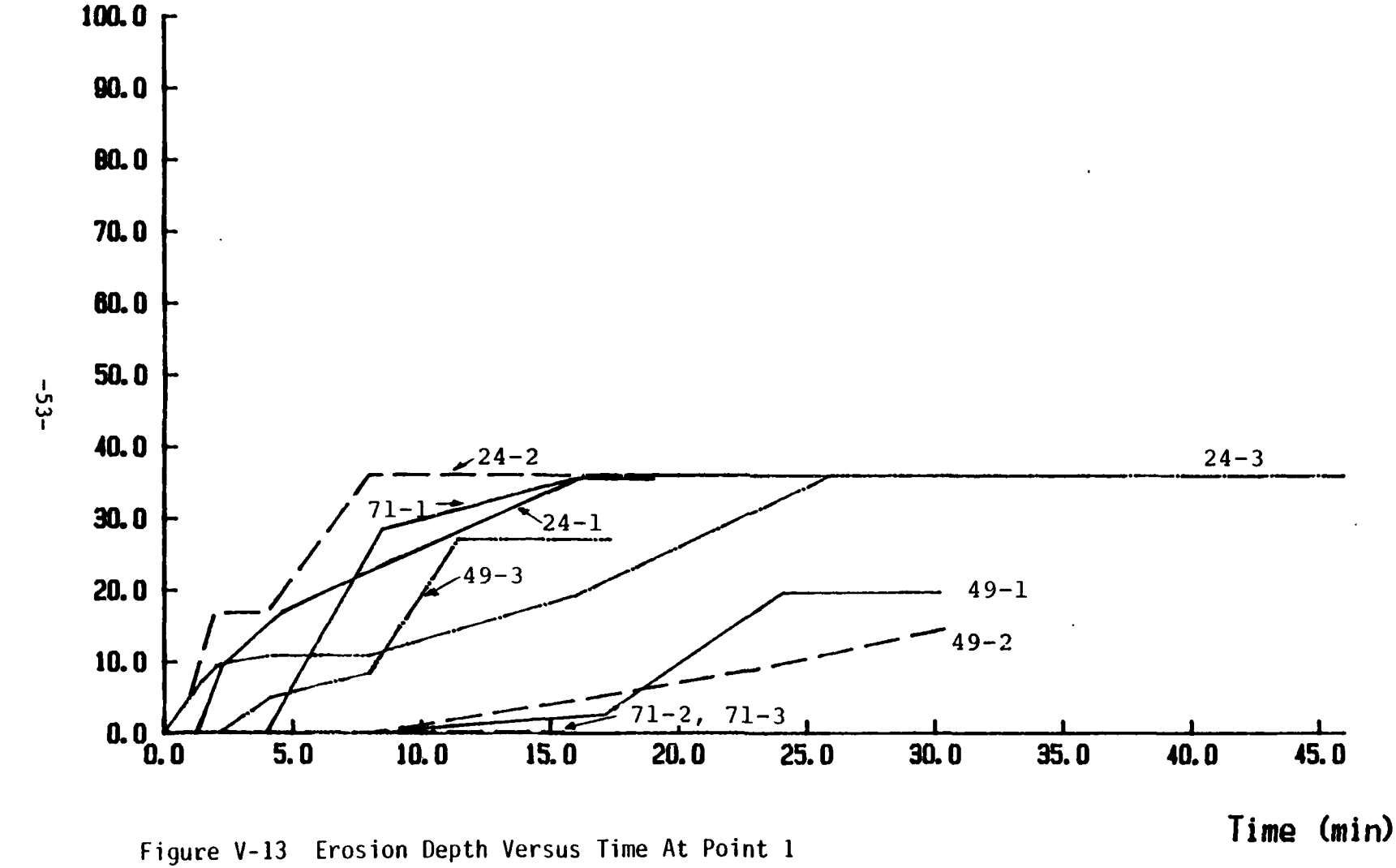

Figure V-13 Erosion Depth Versus Time At Point 1

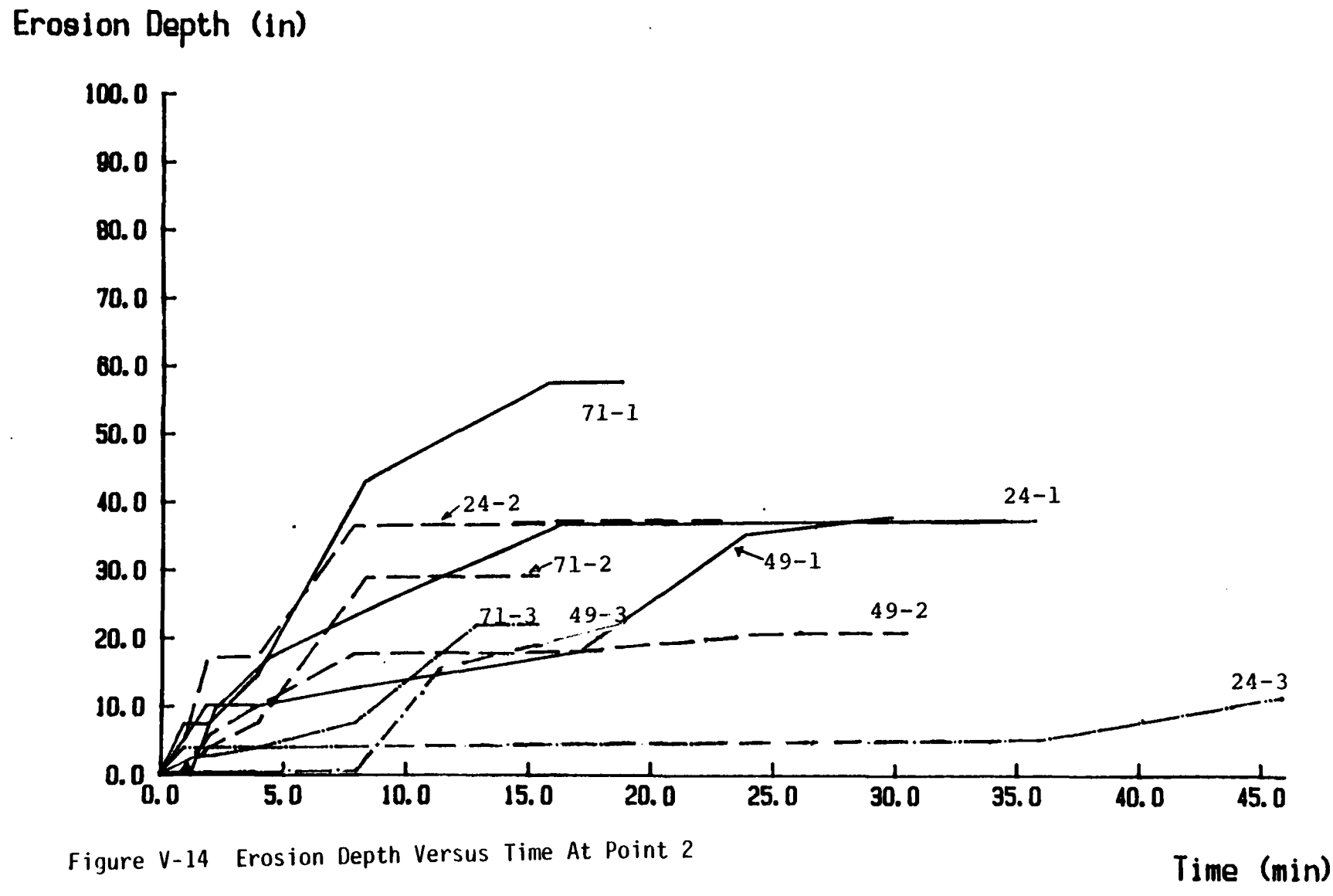

Figure V-14 Erosion Depth Versus Time At Point 2

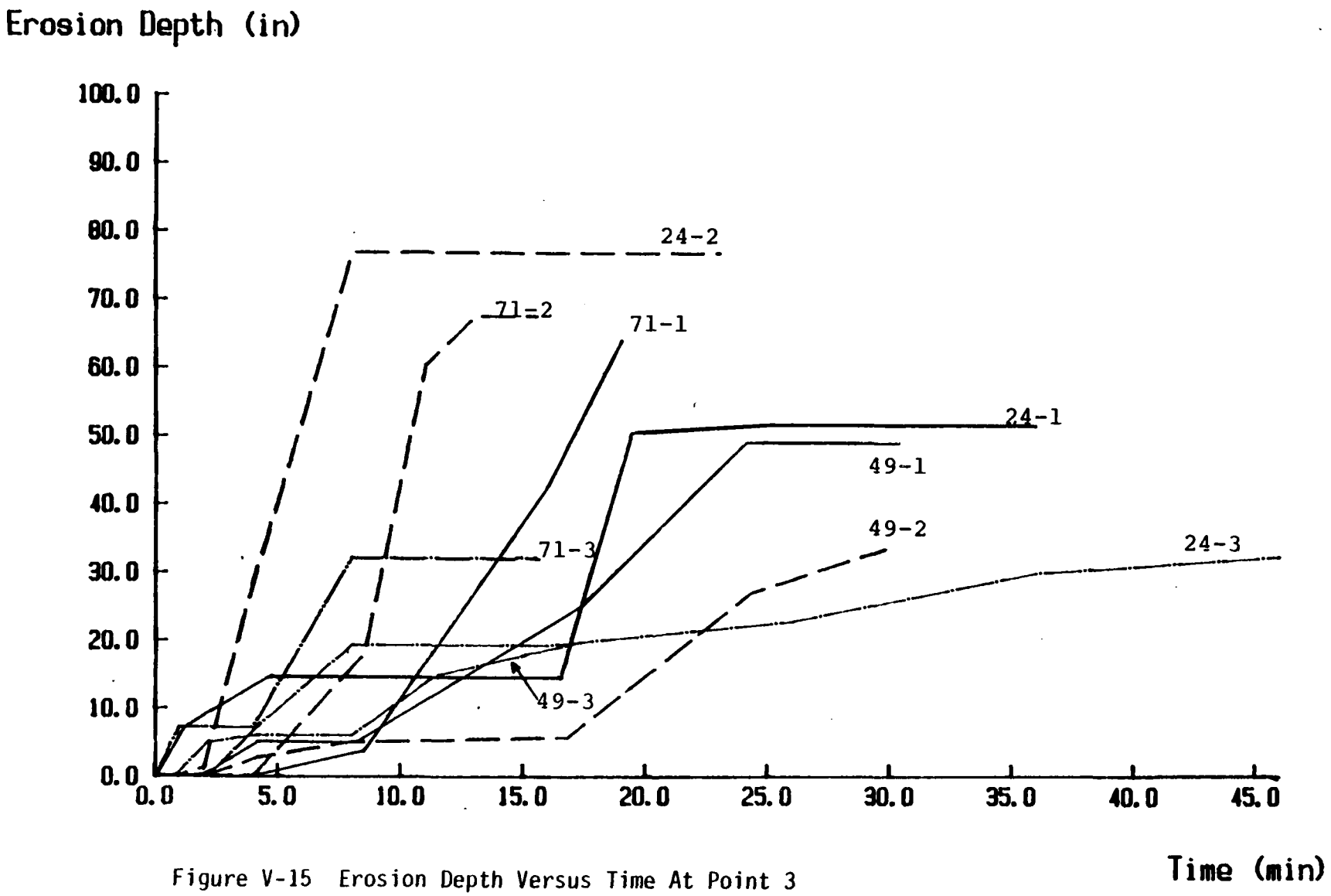

Figure V-15 Erosion Depth Versus Time At Point 3

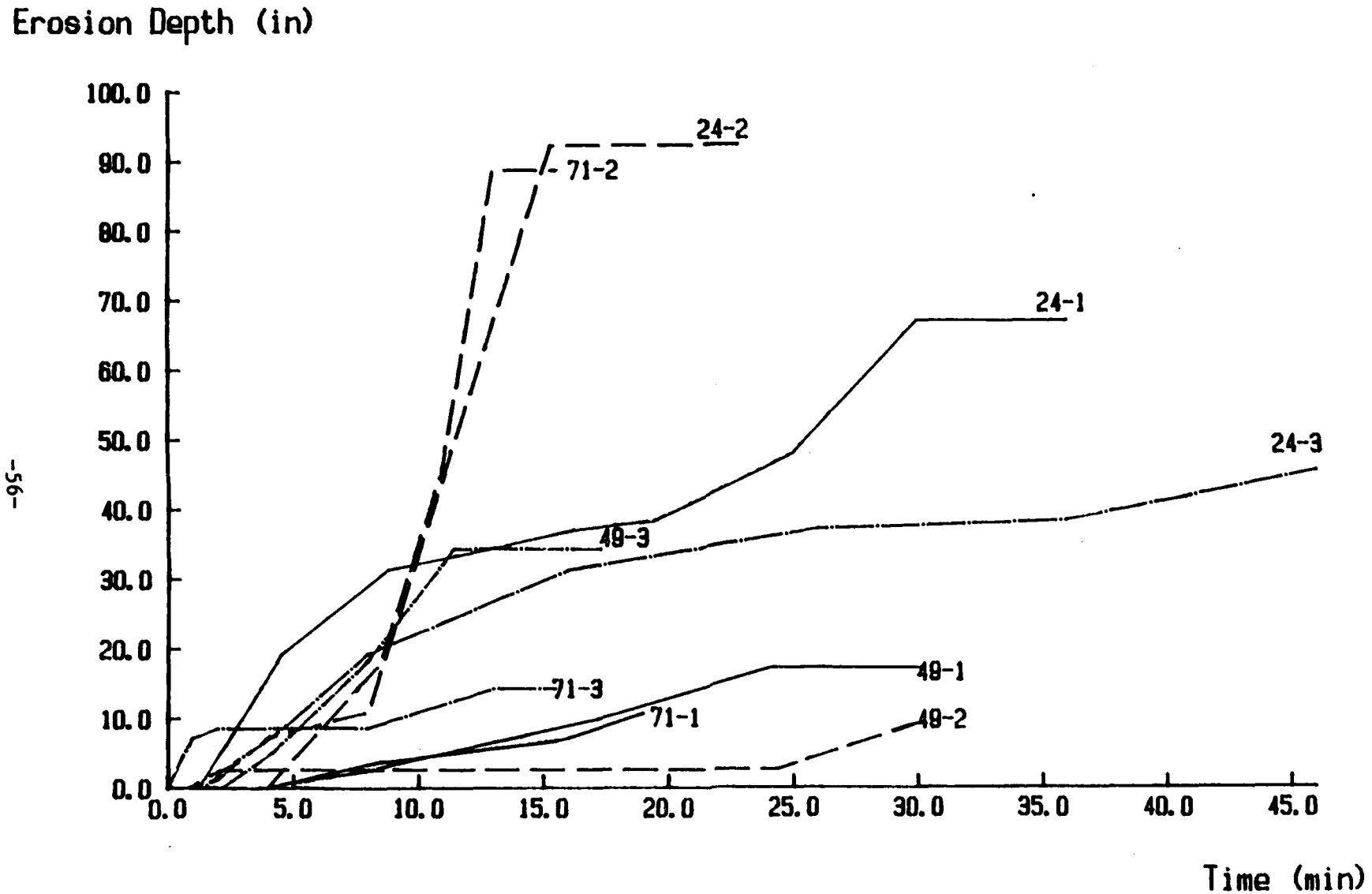

Figure V-16 Erosion Depth Versus Time At Point 4

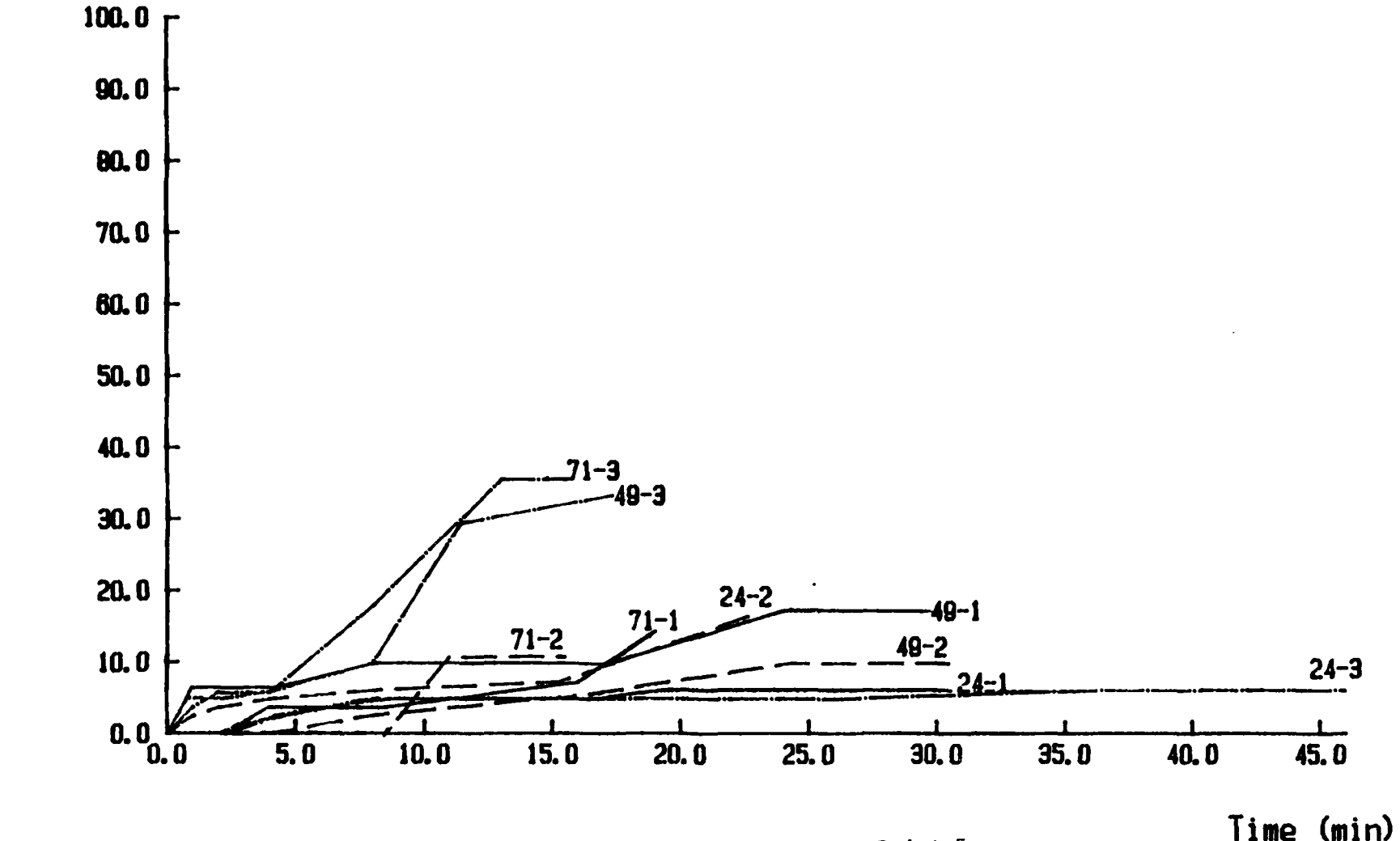

Figure V-17 Erosion Depth Versus Time At Point 5

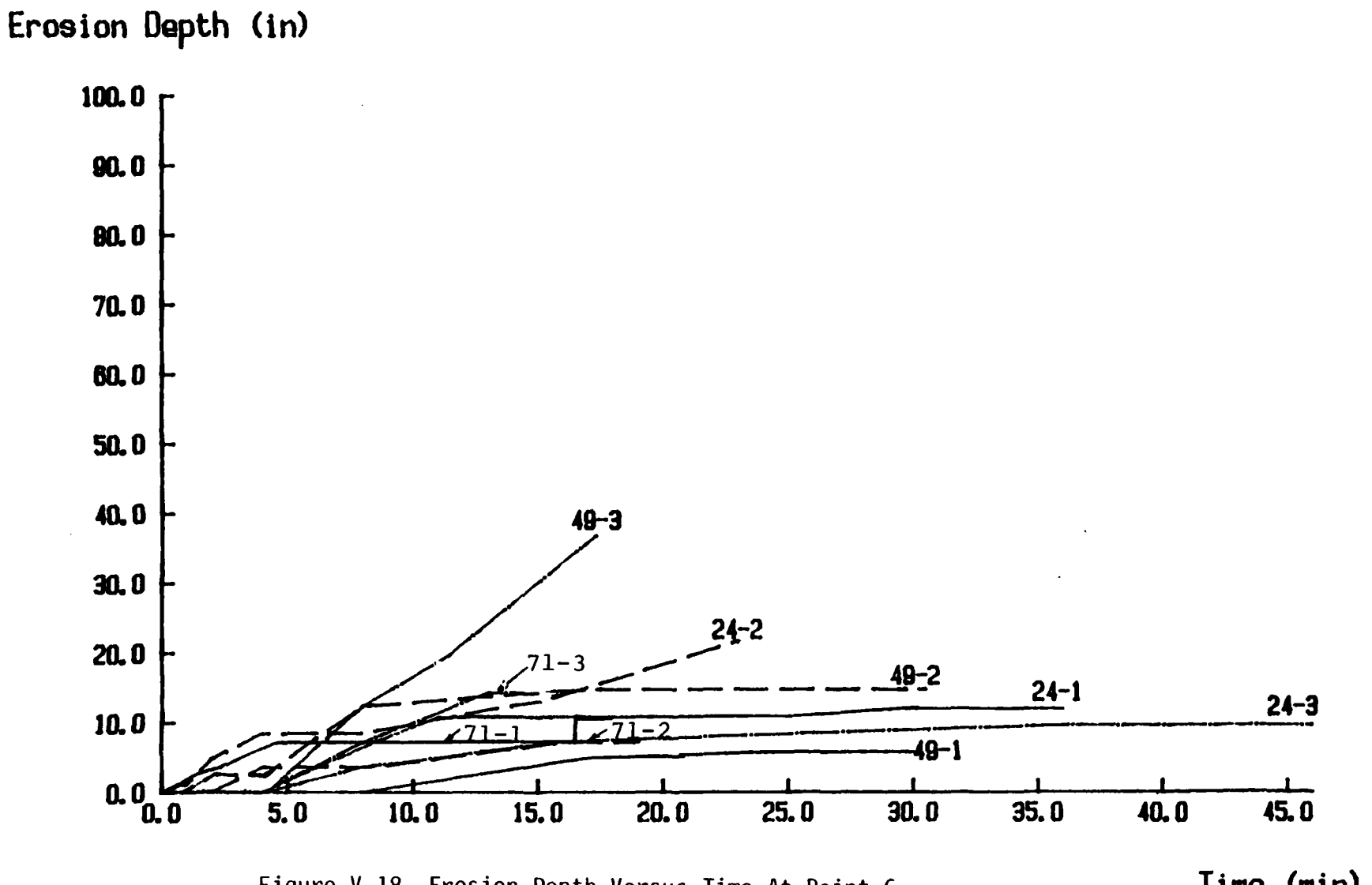

Figure V-18 Erosion Depth Versus Time At Point 6

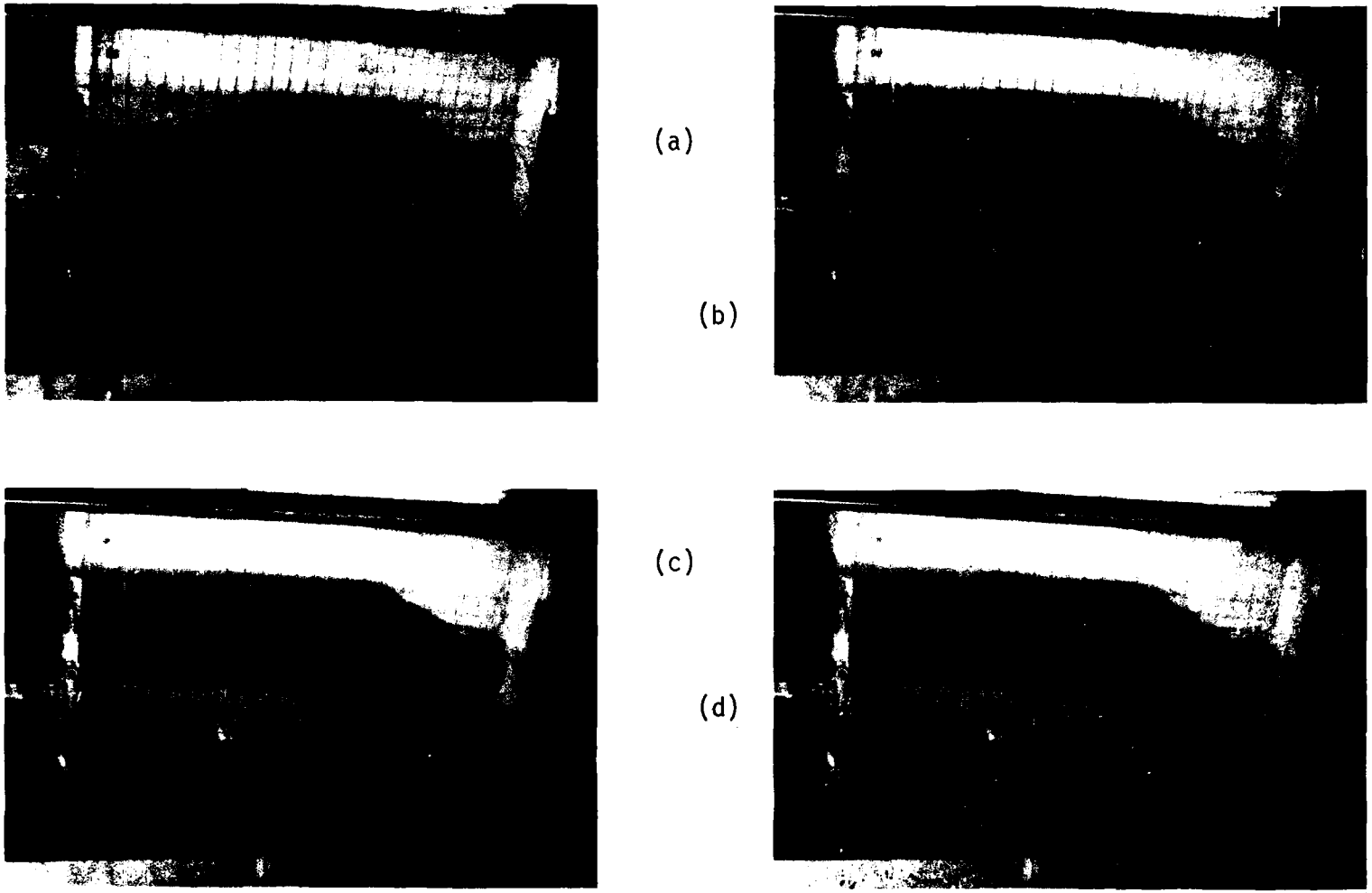

Figure V-19 1/71st Scale Erodable Full Embankment Section: (a) t=0 min. (b) t=1.0 min. (c) t=3.0 min. (d) t=6.0 min.

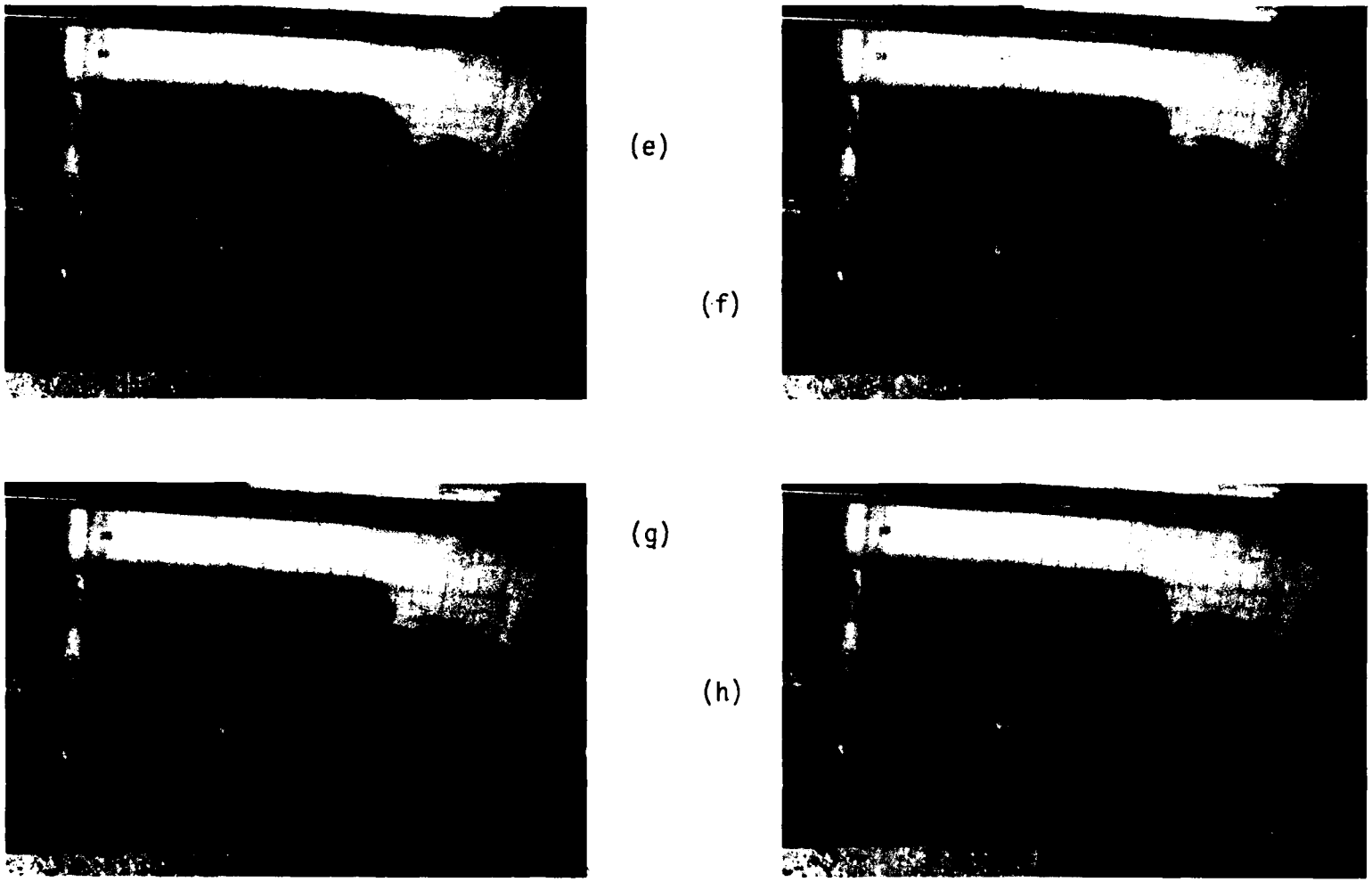

Figure V-19 1/71st Scale Erodable Full Embankment Section: (e) t=9.0 min. (f) t=12.5 min. (g) t=17.0 min. (h) t=21.5 min.

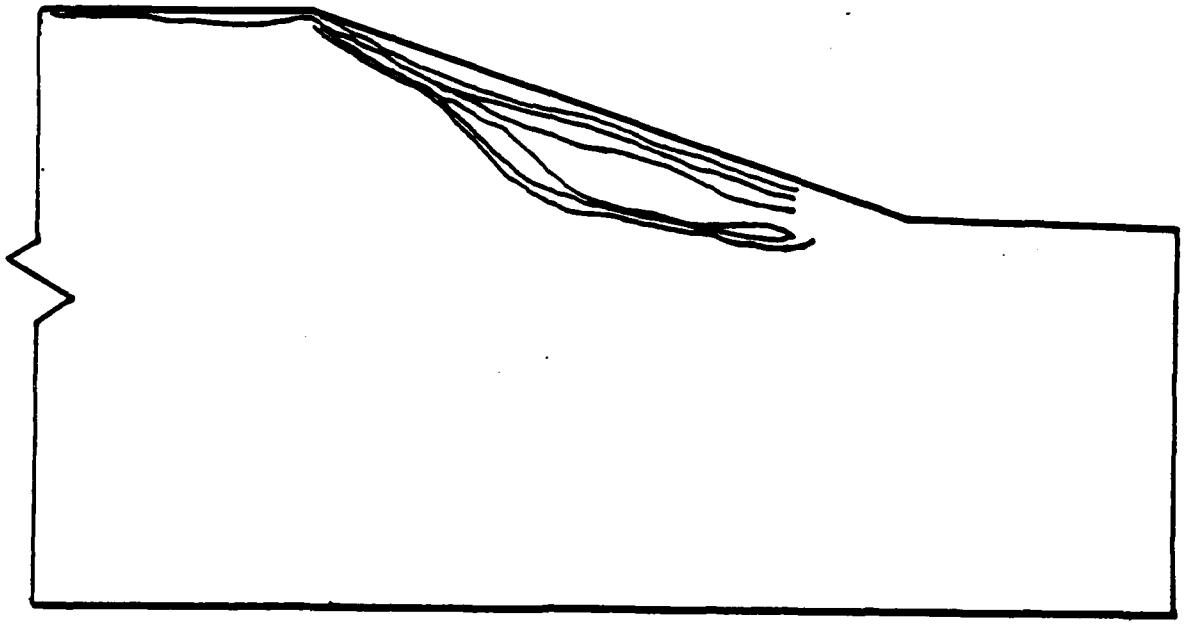

SLA Prototype at 2.5, 5.5, 8.5,13.5, 15.5, and 17.5 hours of Overtopping Flow

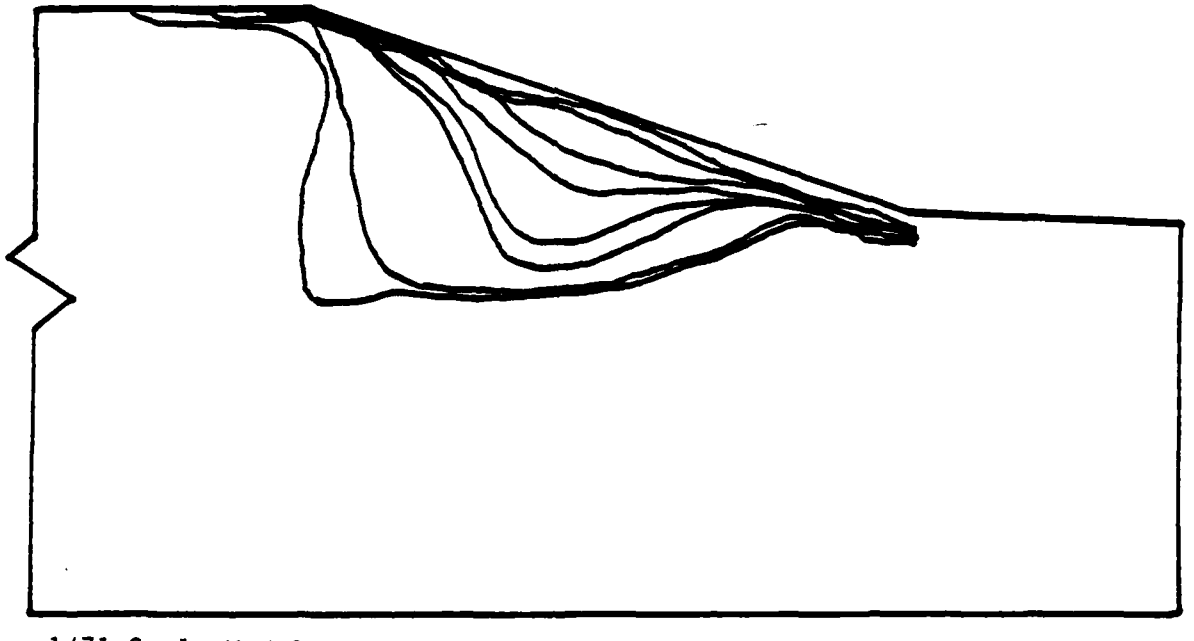

1/71 Scale Model at 1.0, 3.0, 7.2, 8.0, 9.0, 10.0, 14.5, and 19.5 hours of Overtopping Flow (Prototype time)

Figure V-20 Prototype and Full Embankment Model Downstream Slope Erosion Profiles (Scale: 1.0 inch = 6.0 feet, prototype)

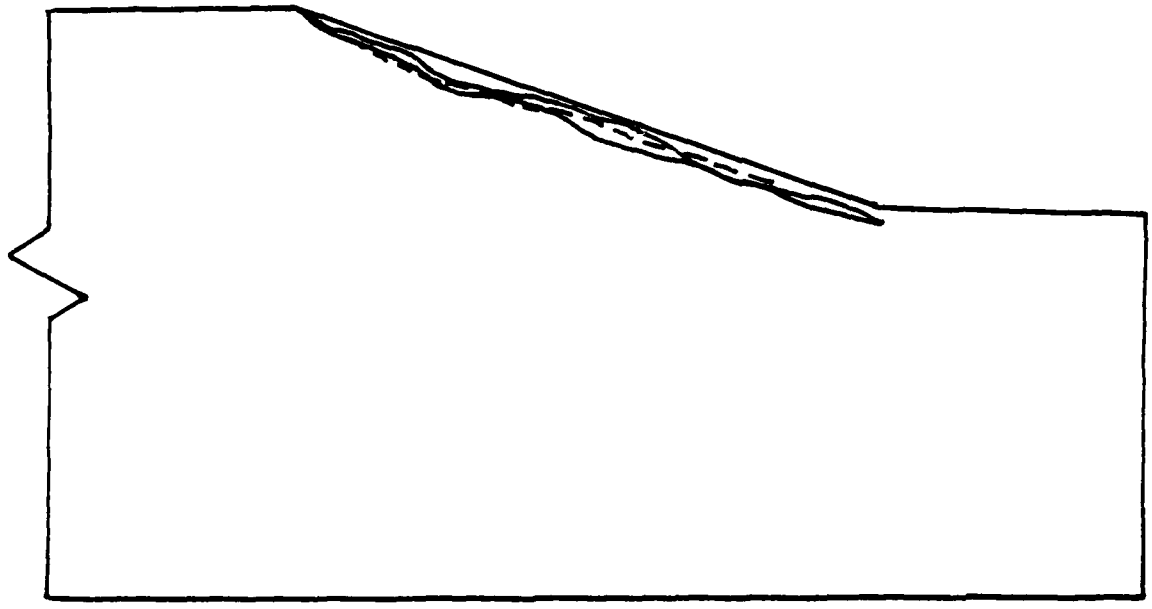

——— 1/71st Scale Model at 1.0 and 3.0 minutes of overtopping

— — — - SLA Prototype at 2.5 hours of overtopping

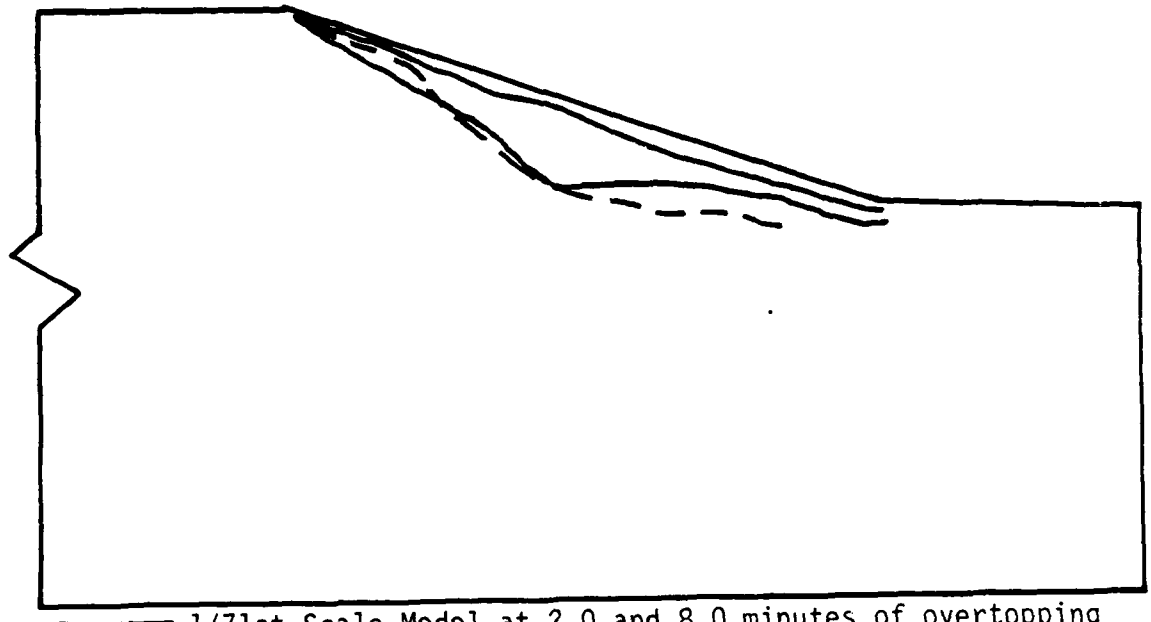

——— 1/71st Scale Model at 2.0 and 8.0 minutes of overtopping

— — — SLA Prototype at 13.5 hours of overtopping

Figure V-21 Prototype and Full Embankment Model Downstream Slope Erosion Profiles (Scale: 1.0 inch = 6.0 feet, prototype)

PART VI: CONCLUSIONS

Phase I - Rigid Embankment Tests

32. In order to show the applicability of the centrifuge to modeling of hydraulic parameters related to open-channel flow a modeling of models analysis was completed on a series of rigid embankments. The results of the analysis indicated that flow quantities q modeled quite well in the centrifuge and the following relationship was determined:

$$q = 0.75\ n\ h^{3/2} \qquad \text{(V-14)}$$

This equation agrees with that presented by Chow (1959) for broad-creased weirs, with the exception that experimental discharge coefficient, 0.75 falls below the range of 2.46 to 3.47 presented by Chow. It is felt that this difference is due to entrance conditions used in the centrifuge models necessitated by the limited space available. These conditions brought about a different ratio of depth of upstream pool to embankment height, and required that overtopping flow had to turn a corner just prior to entering the flow channel. Both of these altered states would change the flow regime upon which Chow's values are based.

Phase II - Erodable Embankment Tests

33. The SLA prototype embankment section was simulated in a modeling of models scheme. The same sandy clay soil was used to construct models at 1/24th, 1/49th, and 1/71st scale which were then tested in triplicates, for a total of nine tests. In all of these models erosion started at the toe and progressed upwards towards the crest, a mechanism like that observed in the feasibility study tests (Ko et al., 1984).

34. Comparison of erosion depth data at various points along the model slopes, indicated a high degree of variability from model to

model, which was attributed to minor variations in density in the models due to preparation techniques and to the random nature of the erosion process. When data on percentage of embankment volume eroded was compared, variability of data was reduced.

35. The modeling of models analysis completed indicated that erosion rates modeled well, and the following relationship for model erosion rate in % vol/min. was determined:

$$\dot{E}_m = 0.0077\, n^{1.38} \qquad \text{(V-15)}$$

The time scaling relationship for erosion was thus found to be:

$$\frac{t_p}{t_m} = n^{1.38} \qquad \text{(V-21)}$$

36. One 1/71st scale full embankment section model was tested and the erosion data was compared to prototype data provided by SLA to evaluate the time scaling relationship. This comparison yielded scaling factors of time of $n^{0.92}$ to $n^{1.18}$, which did not agree with equation V-21. This was likely due in part to variations in the structure of the soil in the model from that in the prototype as a result of variations in compaction technique.

REFERENCES

1. Chow, V.T., Open-Channel Hydraulics, McGraw-Hill, New York, 1959.

2. Ko, H.Y., Dunn, R.J., and Simantob, E., "Study of Embankment Performance During Overtopping and Throughflow," Contract Report for the Department of the Army, Corps of Engineers, Waterways Experiment Station, Contract No. DACW 39-83-C-0011, 1984.

3. Ladd, R.S., "Preparing Test Specimens Using Undercompaction," ASTM Geotechnical Testing Journal, Vol. 1, Mar. 1978, pp. 16-23.